# Two-phase reaction system for efficient photocatalytic production of hydrogen peroxide

Yifan Zhao [a], Yoshifumi Kondo [a], Yasutaka Kuwahara [a,b], Kohsuke Mori [a,b], Hiromi Yamashita [a,*]

[a] *Division of Materials and Manufacturing Science, Graduate School of Engineering, Osaka University, 2-1 Yamadaoka, Suita, Osaka 565-0871, Japan*
[b] *Innovative Catalysis Science Division, Institute for Open and Transdisciplinary Research Initiatives (OTRI), Osaka University, 2-1 Yamadaoka, Suita, Osaka 565-0871, Japan*

## ARTICLE INFO

## ABSTRACT

Hydrogen peroxide ($H_2O_2$) has attracted considerable interest due to its status as an eco-friendly oxidant and a sustainable energy carrier. This review summarizes current advancements in various photocatalysts, including metal-organic frameworks (MOFs), covalent-organic frameworks (COFs), titanium dioxide ($TiO_2$), ionic carbon nitride, quantum dots (QDs), coordination polymer (CP), and heterojunction materials, applied for $H_2O_2$ production in several types of two-phase systems, composed of benzyl alcohol (BA), toluene or octanol organic phase and water phase. Such two-phase media enables spontaneous separation of the produced reduction product ($H_2O_2$) from oxidation product, benzaldehyde (BAL) or octanal and photocatalysts suppressing $H_2O_2$ decomposition. The goal of the present review is to provide more fresh perspective on the future developments in the field of sustainable $H_2O_2$ production in two-phase system.

## 1. Introduction

Hydrogen peroxide ($H_2O_2$), one of the 100 most valuable chemicals in the world [1], is widely used for various purposes due to its oxidizing and disinfectant properties. $H_2O_2$ usually acts as an oxidizing agent in some chemical organic synthesis processes, due to its ability to readily donate oxygen atoms [2]. Especially, $H_2O_2$ is often considered environmentally friendly because of its decomposition into water and oxygen, leaving behind only harmless byproducts, which entitles it to broad applications in wastewater treatment, disinfection [3], and bleaching [4] fields. Recently, $H_2O_2$ has been employed as an energy carrier in a kind of novel single-compartment fuel cell, with a theoretical output potential similar to that of the traditional hydrogen fuel cell [5].

According to the report [6], the global market size of $H_2O_2$ in 2022 was USD 3.07 billion, which grew to USD 3.24 billion in 2023 at a compound annual growth rate (CAGR) of 5.4%. It is expected to increase to USD 4.05 billion in 2027 with a CAGR of 5.7%. In order to meet such growing market demands, some efficient methods have been researched and developed for $H_2O_2$ production.

At present, the oxidation of anthraquinone (AQ) has been a well-established method for $H_2O_2$ synthesis due to its efficiency and ability to generate $H_2O_2$ on a large scale [1,7]. However, process complexity

and waste by-products of AQ oxidation method not only result in substantial energy input but also greatly exacerbate the burden on the natural environment and ecosystems [8]. Therefore, subsequent efforts have been committed to exploring some novel methods for $H_2O_2$ production under more benign conditions and without producing wastes. One alternative method is the direct synthesis of hydrogen ($H_2$) and oxygen ($O_2$) for $H_2O_2$ production, which has the potential to simplify the production process and reduce resource consumption [9]. However, this method requires precise control of reaction conditions, such as a reaction temperature of nearly 0 °C, specific noble metal catalysts, and the ratio of $H_2/O_2$ mixture reaction gas. Despite adding some diluent gases such as carbon dioxide ($CO_2$) and inert gas, the easy explosion property of the $H_2/O_2$ mixture gas limits industrial applications of this reaction process. As a result, there is an urgent need for an ecologically responsible and operationally safe method to generate $H_2O_2$.

Currently, the photocatalytic production of $H_2O_2$ offers a sustainable and direct approach, utilizing renewable solar energy to convert water and oxygen into $H_2O_2$ with high selectivity and minimal resource consumption [10]. Consequently, there has been considerable academic research over the past decade devoted to the advancement of proficient photocatalysts to facilitate the photocatalytic synthesis of $H_2O_2$. These materials encompass diverse entities such as metal-oxide

---

semiconductors [11–14], g-C$_3$N$_4$ [15–18], CdS [19,20], metal-organic complexes [21–24] and covalent organic frameworks [25,26]. As illustrated in Fig. 1a, the mechanism of photocatalytic H$_2$O$_2$ synthesis via the oxygen reduction reaction (ORR) on semiconductor substrates typically encompasses three substantial processes, including light absorption, charge separation, and surface redox reaction [27]. In the first step, the semiconductor irradiated by a light source absorbs protons with greater energy values than the bandgap (E$_g$) of the semiconductor, which activates electrons to transfer from the valence band (VB) to the conduction band (CB). The transition of electrons leaves behind holes with positive charge, which forms electron-hole pairs known as photogenerated charges. Subsequently, photogenerated charges separate and only a minority of them can migrate to the surface of semiconductors whereas most will recombine. The photoinduced electrons and holes, with their respective reducing and oxidizing capabilities, have the potential to propel the redox chemical reactions, provided they can surpass the necessary overpotentials for each electron transfer step, as illustrated in Fig. 1b [28,29].

In an aqueous solution as depicted in Fig. 1c, the separated electrons engage in ORR to generate H$_2$O$_2$, in which oxygen can be reduced via either the indirect stepwise single-electron ORR (1e-ORR) pathway (equations 1 and 2) or a direct one-step two-electron pathway (equation 3). According to the energy diagram shown in Fig. 1b, the 1e-ORR pathway (equation 1) can only proceed when the CB potential of photocatalysts is more negative than -0.33 V versus normal hydrogen electrode (-0.33 V vs. NHE), which involves the formation of superoxide radicals (O$_2^{\bullet-}$) as intermediates. Therefore, the direct 2e-ORR pathway

(0.68 V vs. NHE) exhibits thermodynamical favorability compared to the indirect route (-0.33 V vs. NHE) [30]. On the contrary, the indirect 2e-ORR pathway is more kinetically favored, as each step only requires one single electron [31,32]. Despite this advantage in kinetics, the high reactivity of O$_2^{\bullet-}$, as evidenced by properties of over-reduction and electronic counter-transmission to the photocatalysts, could readily result in the decomposition and limited production of H$_2$O$_2$ [33,34]. Therefore, mitigating this high reactivity of O$_2^{\bullet-}$ would be advantageous to inhibit the decomposition of H$_2$O$_2$ and enhance the effective generation of H$_2$O$_2$ through the indirect ORR route.

For the purpose of enhanced productivity of photocatalytic production of H$_2$O$_2$, various alcohol molecules such as methanol, ethanol [35], isopropanol, benzyl alcohol (BA) [36], etc. are often introduced into the photoreaction system as sacrificial agents. They are used to quench photogenerated holes, thus donating more electrons to the ORR process. Shiraishi et al. [37] reported the superiority of BA molecules as electron donors in H$_2$O$_2$ formation compared to aliphatic alcohols, which is attributed to the efficient formation of peroxo species, readily transforming to H$_2$O$_2$. The synthesis of H$_2$O$_2$ is followed by the alcohol oxidation reaction process to produce another high-value compound, benzaldehyde (BAL) (1.98 V vs. NHE) (equation 4), with R representing the benzene ring, in the same solution. However, the H$_2$O$_2$ decomposition, caused by direct contact between the formed H$_2$O$_2$ and semiconductors, is so difficult to avoid in the single-liquid phase solution and leads to the hampered productivity of H$_2$O$_2$. Besides, the separation of H$_2$O$_2$ and BAL products in a single phase requires significant energy consumption and additional economic expenses.
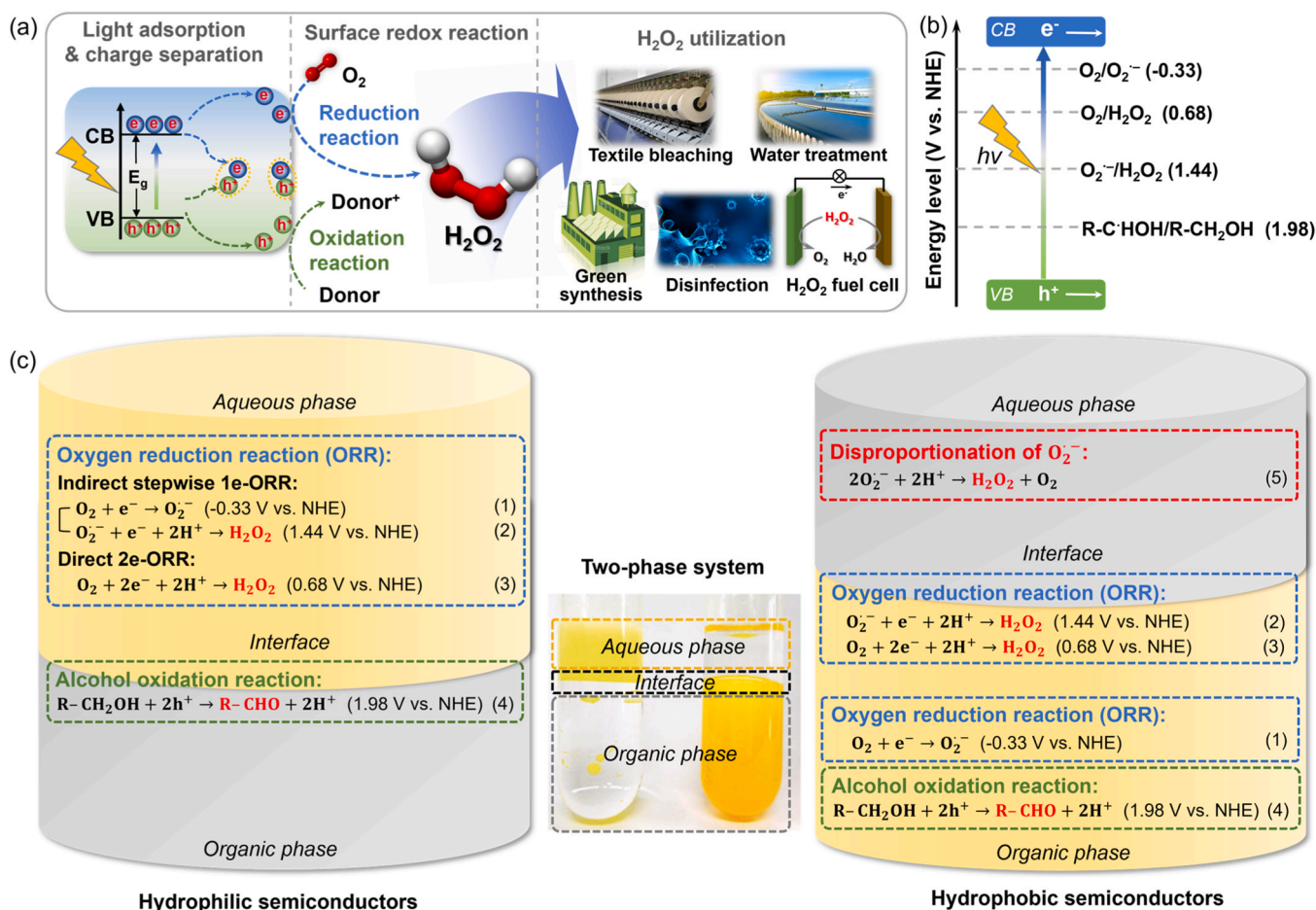


**Fig. 1.** (a) Schematic illustration of the photocatalytic processes for H$_2$O$_2$ production and the use of H$_2$O$_2$. (b) Energy level diagram for biphasic photocatalytic H$_2$O$_2$ production via ORR and alcohol oxidation routes using a semiconductor. (c) Reaction mechanism diagram of two-phase (aqueous/organic phase) photocatalysis using hydrophilic and hydrophobic catalysts, respectively, involved in ORR and alcohol oxidation reactions.

In 2019, our group first presented the hydrophobized metal-organic frameworks (MOFs) applied in a two-phase system for photocatalytic $H_2O_2$ production, involving water and BA solvents, which enables $O_2^{\bullet-}$ to separate from the photocatalysts and efficiently suppresses the $H_2O_2$ decomposition [21]. Furthermore, the design of the BA/water system is rooted in the considerations of economically coordinated processes and the challenges posed by product separation. The reaction mechanism within such a two-phase system diverges slightly from that observed in a single liquid-phase environment. Specifically, as described in Fig. 1c, for hydrophilic photocatalysts, the oxidation process involving their photoinduced holes is dominated by the oxidation reaction of BA (equation 4) occurring at the interface between water and the organic solution. Conversely, with hydrophobic semiconductors employed in the two-phase setup, the $O_2^{\bullet-}$ species resulting from the indirect 1e-ORR (equation 1) migrate to the aqueous phase. They initiate the disproportionation process (equation 5) for $H_2O_2$ production in the aqueous medium, while the produced BAL remains confined in the organic solvent phase.

In such a two-phase system, the photocatalysts are designed to maintain stably within the organic phase, which suppresses the $H_2O_2$ decomposition and facilitates the $H_2O_2$ production in the aqueous phase. Therefore, the optimal hydrophobicity of diverse materials plays a critical role in enhancing the $H_2O_2$ production efficiency in this biphasic reaction, which is reflected in the observation that excessive hydrophobicity in catalysts might adversely affect the adsorption and mass transportation of $O_2$ molecules on their surface in the organic phase [38, 39]. Except for inherently hydrophobic materials, some methods of hydrophobic modification were summarized in this review, such as alkylation on linkers and metal clusters of MOFs [21,22,40,41], as well as alkyl-silanization on hydrophilic semiconductors [42].

Until now, there has been a surge in studies focused on the photocatalytic production of $H_2O_2$ within the aqueous/organic biphasic system, which is composed of water and aromatic compounds or aliphatic alcohol. This review summarized various materials hitherto used in several innovative two-phase reaction systems, including MOFs, covalent organic frameworks (COFs), titanium dioxide ($TiO_2$), quantum dots, coordination polymer, and heterojunction, and their improvement on the $H_2O_2$ production efficiency. The present review aims to broaden valuable insights concerning advancements in the realm of hydrophobic photocatalysts and the strategic formulation of reaction systems for photocatalytic $H_2O_2$ production.

## 2. Benzyl alcohol/water phase

### 2.1. Metal-organic frameworks (MOFs)

Metal-organic frameworks (MOFs), as a class of porous materials with unique structures, consist of metal ions or clusters bonded to organic ligands, which create two- or three-dimensional networks with nanoscale-sized pores [43,44]. Thanks to the features of exceptional surface area ($> 1000$ $m^2$ $g^{-1}$), high porosity, and tuneable properties, MOFs are known as versatile materials for various applications, including gas storage and separation, catalysis, drug delivery, and sensors [45]. Notably, the functionalization of MOFs has attracted much interest in the field of photocatalysis. For instance, hydrophobic modification in the ligands or metal-oxo clusters of MOFs imparts hydrophobic properties to some initially hydrophilic MOFs, such as MIL-125-$NH_2$ and UiO-66-$NH_2$ which contain amine groups [46,47]. For photocatalytic $H_2O_2$ production in a two-phase system, the advancements of hydrophobic MOFs to enhance $H_2O_2$ production are reviewed as follows.

### 2.1.1. Linker hydrophobization of MOFs

Grafting long alkyl chains onto the linker of MOFs can significantly enhance the hydrophobic characteristics of MOFs. Our group modified MIL-125-$NH_2$, a kind of Ti-based MOFs composed of $Ti_8O_8(OH)_4$ clusters

interconnected by 2-aminoterephthalate linkers, with alkyl chains of different lengths as shown in Fig. 2a [21]. The MOF with alkylated linkers is denoted as MIL-125-Rn, where n is the number of carbon atoms in the alkyl chain (4 or 7).

At first, on the basis of X-ray diffraction (XRD), scanning electron microscopy (SEM) and transmission electron microscopy (TEM) results, the authors conclusively established that the original crystal structure and morphology of MIL-125-$NH_2$ remained barely altered, even after the incorporation of alkyl chains in the linker-alkylated MIL-125-Rn. Additionally, the quantification of alkyl chains within MIL-125-Rn was achieved through thermogravimetric (TG-DTA) analysis, which could be calculated as 61% in MIL-125-R4 and 59% in MIL-125-R7, respectively. Water contact angle measurement (embedded graphs of Fig. 2a) was performed to estimate the hydrophilicity/hydrophobicity of MIL-125-$NH_2$ and MIL-125-Rn. MIL-125-Rn exhibits hydrophobic with the water contact angles of 101° (n=4) and 124° (n=7), whereas MIL-125-$NH_2$ shows hydrophilic with that of 30°. MIL-125-$NH_2$ only existed in an aqueous solution of the BA/water two-phase reaction system (Fig. 2b, left), in which $H_2O_2$ production exclusively occurred under visible-light irradiation of $\lambda > 420$ nm. As expected, MIL-125-R7 dispersed selectively in the BA phase (Fig. 2b, right) with highly improved $H_2O_2$-producing rate and activity for photocatalytic $H_2O_2$ synthesis (Fig. 2c). Moreover, the $H_2O_2$ concentration exhibited an inverse relationship with the volume of the aqueous phase, with the optimal ratio being 2:5 (water/BA, mL/mL) compared to ratios of 5:5 and 10:5. It indicates that the two-phase system allows for the easy concentration of the produced $H_2O_2$ during its production.

Ultimately, the authors attribute such a huge difference in $H_2O_2$ production to the discrepancy in the capacity for $H_2O_2$ decomposition. When $H_2O_2$ and MIL-125-$NH_2$ are in the same phase, produced $H_2O_2$ will be photo-reduced into $OH^-$ and $^{\bullet}OH$, which eventually leads to the stagnation of $H_2O_2$ production [48]. Therefore, utilization of alkylated MOFs MIL-125-Rn in the two-phase system provides a promising thought for suppressing photocatalytic decomposition of $H_2O_2$, resulting from the partial separation of $H_2O_2$ and photocatalysts. On the other hand, the design of this two-phase system allows for the retention of active $O_2^{\bullet-}$ intermediates, which act as the reactant of disproportionation of $O_2^{\bullet-}$ to $H_2O_2$ reaction [33]. In detail, it is reported that $O_2^{\bullet-}$ species become more stable to facilitate the formation of $H_2O_2$ under low pH conditions [49,50], in which the structure of MIL-125-$NH_2$ will be destroyed because of the detachment of the terephthalate linkers. Nevertheless, this limitation of MOFs stability could be broken by considering MIL-125-Rn, as it only resides in the BA phase (Fig. 2d). Higher $H_2O_2$ concentration was observed with increasing pH values in the aqueous phase of the two-phase setup, with peak activity at pH 0.3. Additionally, employing saturated NaCl solution as the aqueous phase led to enhanced production for $H_2O_2$. This notable surge in activity can be attributed to the isolation of MIL-125-Rn from the low-pH aqueous phase, where the disproportionation of $O_2^{\bullet-}$ to $H_2O_2$ efficiently occurs, alongside the strong complexation of $O_2^{\bullet-}$ with $Na^+$ Lewis acid, resulting in heightened stabilization of $O_2^{\bullet-}$ radicals.

### 2.1.2. Hydrophobic modification to metal clusters in MOFs

Although the MIL-125-R7 exhibited a fourfold increase in photocatalytic activity of $H_2O_2$ synthesis within this two-phase system compared to MIL-125-$NH_2$ (Fig. 2c), the long chain alkylation on the linker resulted in a noteworthy decrease in the Brunauer-Emmett-Teller (BET) surface area of MIL-125-R7 (561 $m^2$ $g^{-1}$), while that of MIL-125-$NH_2$ is 1498 $m^2$ $g^{-1}$. Thus, if the high BET surface area of MIL-125-$NH_2$ can be maintained after alkylation, it is expected that much higher activity can be achieved.

Accordingly, our group devised an alternative hydrophobic MOF named OPA/MIL-125-$NH_2$, where the Ti metal clusters were alkylated using octadecyl-phosphonic acid (OPA) [40]. In contrast to MIL-125-R7, where the alkyl chains grafted onto the linkers occupied some pores (Fig. 3a, top), the alkylation using OPA (OPA/MIL-125-$NH_2$) selectively
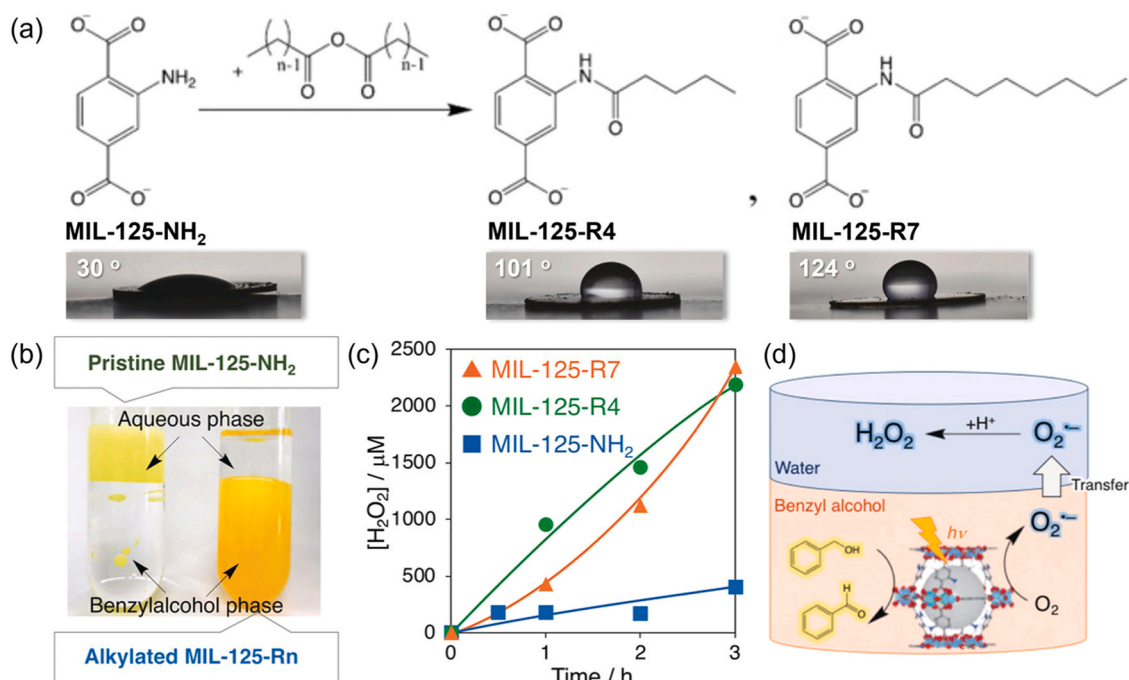
**Fig. 2.** (a) Synthesizing process and water contact angles of MIL-125-Rn (n = 4 or 7) generated by linkers alkylation reaction of MIL-125-NH$_2$. (b) Digital photograph and (c) H$_2$O$_2$ concentration under photoirradiation ($\lambda$ > 420 nm) in the two-phase system. (d) Proposed schematic diagram of photocatalytic H$_2$O$_2$ synthesis in the two-phase system. Reproduced with permission from ref. [21].
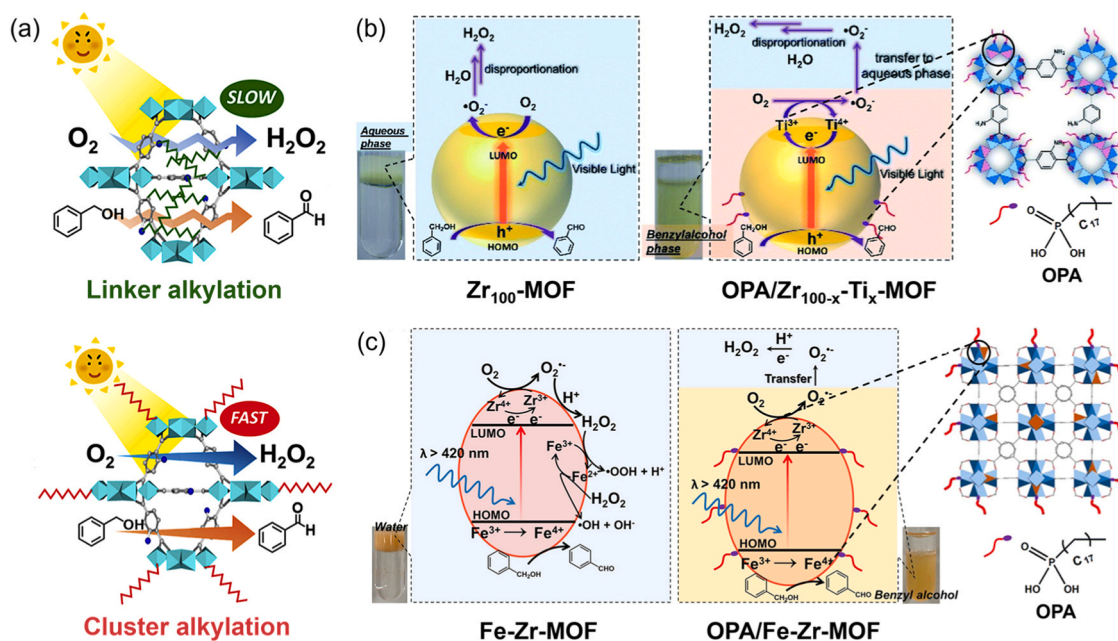


**Fig. 3.** (a) Model diagram of linker-alkylated MOFs (MIL-125-Rn) and cluster-alkylated MOFs (OPA/MIL-125-NH$_2$). [40]. Illustrations showing the use of hydrophobic (b) OPA/Zr$_{100-x}$-Ti$_x$-MOF (Reproduced with permission from ref. [22]) and (c) OPA/Fe-Zr-MOF for photocatalytic H$_2$O$_2$ production in the water/BA two-phase reaction system (Reproduced with permission from ref. [41]).

modified the outermost surface of MIL-125-NH$_2$ by targeting only the Ti$_8$O$_8$(OH)$_4$ clusters with open coordination sites, thereby preserving most of the pores (Fig. 3a, bottom) as evidenced by the fact that BET surface area of OPA/MIL-125-NH$_2$ is 1242 m$^2$ g$^{-1}$, which is similar to original MIL-125-NH$_2$. Under visible light irradiation, the employment of OPA/MIL-125-NH$_2$ in the two-phase system as a photocatalyst for H$_2$O$_2$ production was conducive to facilitating the production rate of H$_2$O$_2$, reaching 853 μmol h$^{-1}$ g$^{-1}$ at a catalyst concentration of 1 mg/mL

in a BA/water ratio of 5:2 solution, compared to when MIL-125-R7 was employed. The authors explained that this improvement was attributed to the fast diffusion of reactant and product molecules through the open pores of OPA/MIL-125-NH$_2$, leading to the accelerated BA oxidation reaction and halted decomposition of H$_2$O$_2$.

Based on the advantage of cluster-hydrophobization of Ti-based MOFs, including boosting the mass transfer of molecules, our group subsequently extended the versatility of this approach to another type of

MOFs, Zr-based MOFs, which feature excellent structural stability and high porosity [51–53]. In particular, it is reported that UiO-66-NH$_2$ as a typical Zr-MOF, composed of Zr oxo clusters and 2-aminoterephthalate linkers, has attracted much attention in the field of catalysis. Moreover, doping some suitable metal ions into Zr oxo clusters, serving as electron mediators through substitution of partial Zr$^{4+}$ ions in Zr-MOFs, is able to enhance the charge separation and mitigate the recombination of photoinduced electrons and holes within the MOF matrix [54].

Owing to the similar chemical properties between Zr$^{4+}$ and Ti$^{4+}$, as well as the fact that Ti$^{4+}$ effectively acts as active sites in the photocatalytic reactions [55,56], our group launched a series of hydrophobic Ti-doped UiO-66-NH$_2$ catalysts modified with OPA (OPA/Zr$_{100-x}$Ti$_x$--MOF) as present in Fig. 3b [22]. The Ti$^{4+}$-doping helps to suppress the recombination of photogenerated electrons with holes, achieved through the redox reaction of Ti$^{4+}$/Ti$^{3+}$. Doped Ti$^{4+}$ ions within clusters capture the photoexcited electrons in the lowest unoccupied molecular orbital (LUMO) of OPA/Zr$_{100-x}$Ti$_x$-MOF. Subsequently, they are reduced to Ti$^{3+}$ followed by O$_2$ reduction to produce O$_2^{\bullet-}$ species for H$_2$O$_2$ synthesis. Simultaneously, the holes residing in the highest occupied molecular orbital (HOMO) are effectively extinguished through the oxidation of BA. Therefore, this Ti$^{4+}$-doping strategy plays a crucial role in improving the ligand-cluster charge transfer (LCCT) of MOFs, which results in a remarkably promoted activity. The BA/water two-phase system, which enables the transfer of O$_2^{\bullet-}$ into an aqueous phase separated from the catalysts, also contributes to improved catalytic performance by suppressing H$_2$O$_2$ decomposition.

Furthermore, our group conducted research about OPA-modified Fe$^{3+}$-doped Zr-MOF (OPA/Fe-Zr-MOF) for photocatalytic synthesis of H$_2$O$_2$ as illustrated in Fig. 3c [41], based on the fact that the electron-donating properties of Fe$^{3+}$ to enhance the metal-to-cluster charge transfer (MCCT) [57]. Fe$^{3+}$-doping enables UiO-66 Zr-MOF

with visible-light response obtained by UV–vis DRS measurement and to generate electrons for reduction of Zr$^{4+}$ species in clusters to Zr$^{3+}$ species. Subsequently, the generated electrons are used for the reduction of adsorbed O$_2$ to O$_2^{\bullet-}$ species through the redox of Zr$^{4+}$/Zr$^{3+}$, while formed Fe$^{4+}$ species from Fe$^{3+}$ are quenched through the oxidation of BA in the two-phase system. In the aqueous phase, for hydrophilic Fe-Zr-MOF, H$_2$O$_2$ is produced via the reaction of O$_2^{\bullet-}$ with protons. Unfortunately, the formed H$_2$O$_2$ will be consumed because of the Fenton-like reaction induced by Fe$^{3+}$ ions, in which Fe$^{3+}$ reacts with H$_2$O$_2$ to yield superoxide species ($^{\bullet}$OOH) and hydroxyl radicals ($^{\bullet}$OH). As for the hydrophobic OPA/Fe-Zr-MOF, the spatial separation of OPA/Fe-Zr-MOF in the BA phase from H$_2$O$_2$ in the aqueous phase effectively inhibits the Fenton-like reaction, thereby preventing the consumption of H$_2$O$_2$.

### 2.2. Covalent-organic frameworks (COFs)

Recently, in contrast to MOFs, a novel class of metal-free crystalline porous organic polymers, known as covalent organic frameworks (COFs), has gained prominence as potential photocatalysts owing to their expansive surface areas, remarkable structural tunability, visible-light harvesting properties, and promising stability [58–60]. To date, a few COFs, such as those based on triphenyl-benzene [61], triazine [62], bipyridine [63], and vinylene-linked triazine [64], have been explored for their potential in photocatalytic H$_2$O$_2$ production. These COFs have exhibited heightened photo-activity for H$_2$O$_2$ synthesis, primarily attributed to their exceptionally porous conjugated frameworks coupled with their capacity for structural customization and designability. Inspired by the design of the binary BA/water system mentioned above, several researchers have directed their efforts towards utilizing hydrophobic COFs in the context of photocatalytic H$_2$O$_2$ production within a two-phase system.
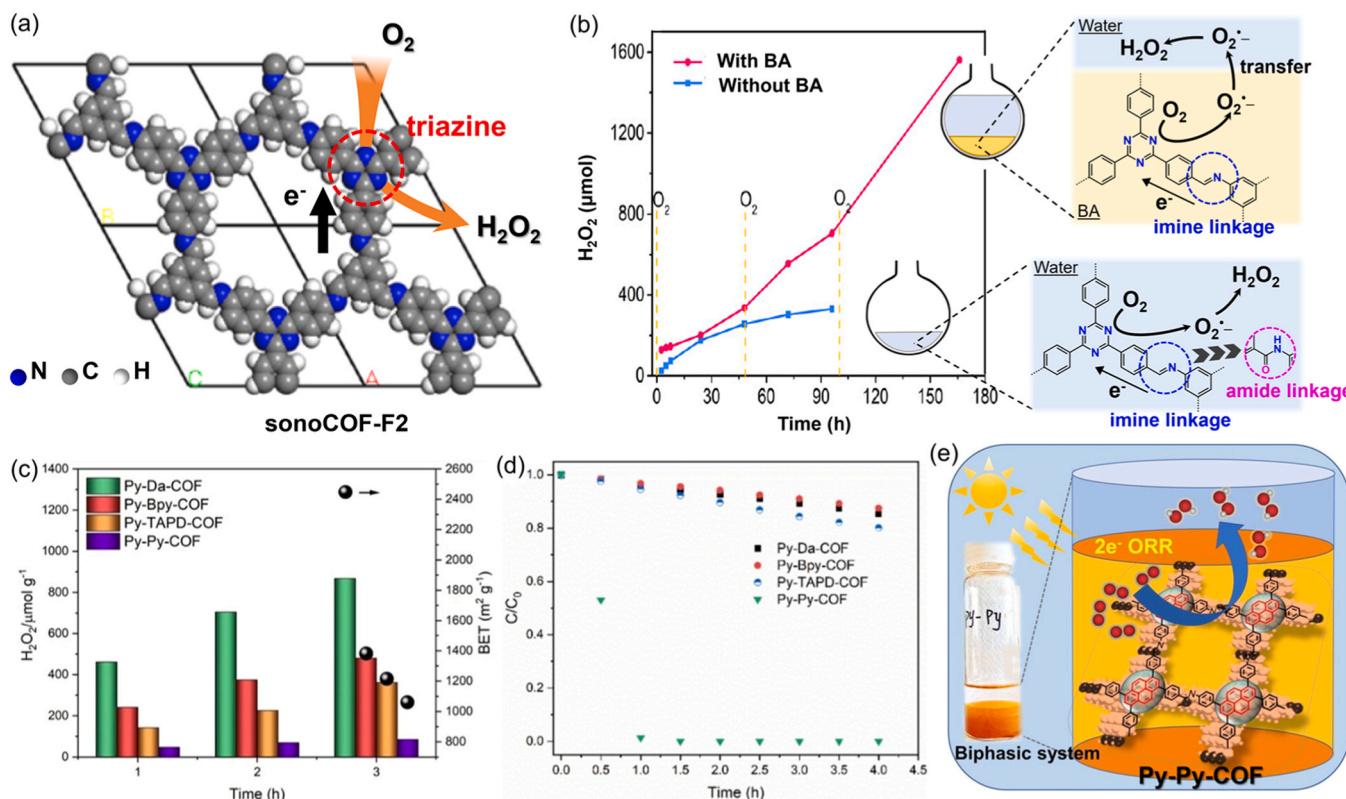


**Fig. 4.** (a) Proposed schematic for the photocatalytic formation of H$_2$O$_2$ using the triazine-containing COF (sonoCOF-F2). (b) The H$_2$O$_2$ concentration during long-term stability test and reaction mechanism of sonoCOF-F2 for photocatalytic H$_2$O$_2$ production in aqueous phase and two-phase systems. Reproduced with permission from ref. [65]. (c) Photoactivity of pyrene-based COFs for H$_2$O$_2$ production in water. (d) Time course of H$_2$O$_2$ decomposition on COFs under light irradiation. (e) Schematic diagram for photocatalytic H$_2$O$_2$ synthesis of Py-Py-COF in a biphasic system. Reproduced with permission from ref. [68].

Zhao et al. [65] developed an imine-based COF (sonoCOF-F2) containing triazine units as shown in Fig. 4a, which displayed considerable photoactivity in the synthesis of $H_2O_2$. Specifically, the triazine unit of sonoCOF-F2, composed of three nitrogen atoms, gave rise to a configuration with both electron-rich and electron-poor sites. This unique arrangement contributed to enhanced charge separation and subsequently resulted in superior photocatalytic activity when compared to the benzene-containing COFs. However, during a long-term stability test exceeding 96 h in a pure water solvent, the $H_2O_2$ yield catalyzed by sonoCOF-F2 gradually declined due to the transformation of imine linkages into amide linkages within the COFs, which results in weakened crystallinity and electronic conjugation (Fig. 4b). To address this problem of imine inactivation, a BA/water two-phase system was employed, in which the COFs remained in the BA phase, with the solid solution ratio of 6 mg/mL, while the produced $H_2O_2$ in aqueous phase. The authors also observed that higher volume ratio of BA/water phases (9:1) contributes to an increased $H_2O_2$ concentration rate (414.6 mmol h$^{-1}$ g$^{-1}$), resulting from the higher dispersion of catalysts in the BA phase. Therefore, this two-phase system not only proficiently shields the

imine-based COFs catalysts from oxidation caused by photogenerated holes or $O_2^{\bullet-}$ radicals into inactive amide-linked COFs, but it also allows for the spontaneous segregation of the $H_2O_2$ and BAL products.

In addition to the electron-rich interaction of triazine moiety showing superior catalytic performance for the biphasic photocatalytic synthesis of $H_2O_2$, the pyrene-based COFs also have been studied due to their stacked π-π conjugate structure, resulting in a narrower band gap for COFs, and pyrene units are regarded as active reduction centres [66, 67]. Inspired by the features of pyrene, Sun et al. [68] designed four imine-linked COFs with different π-conjugated intensities, in which Py-Py-COF with pyrene units shows similar surface areas and most active pyrene units. However, the Py-Py-COF exhibited lower photoactivity under irradiation of λ > 420 nm in the aqueous phase compared to other pyrene-contained COFs with less pyrene units as present in Fig. 4c. The authors conclude that the generated $H_2O_2$ undergoes decomposition on the surface of Py-Py-COF rather than diffuses into water, as supported by the notably rapid decomposing rate of $H_2O_2$ observed in Fig. 4d. Therefore, the closely spaced and abundant pyrene active sites within Py-Py-COF induce undesired decomposition of $H_2O_2$,
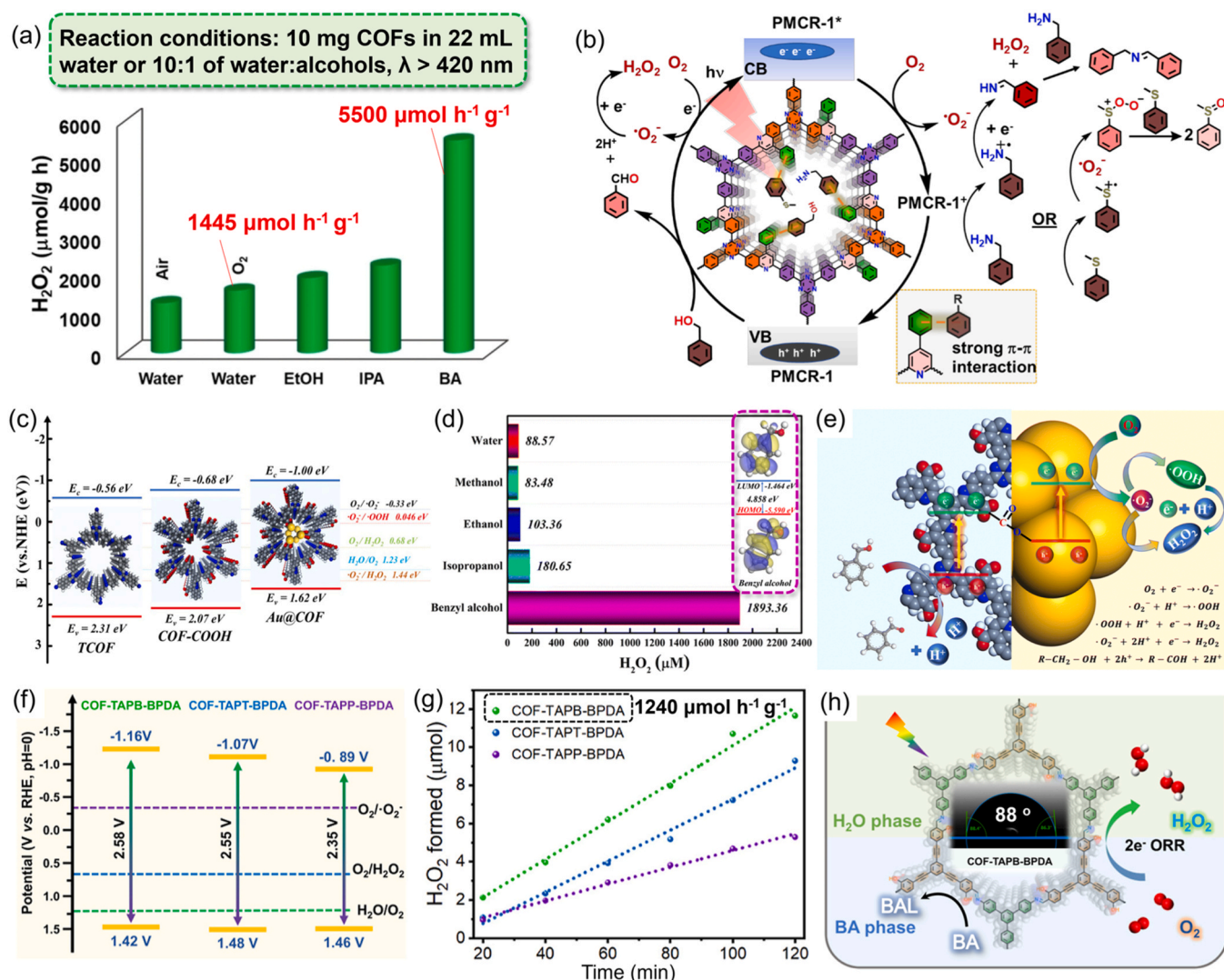


**Fig. 5.** (a) Photocatalytic $H_2O_2$ production rate using PMCR-1 COF in water or water with different sacrificial agents. (b) Reaction mechanism catalyzed by PMCR-1 with different electron donors. Reproduced with permission from ref. [70]. (c) Band structure diagram of TCOF, COF-COOH, and Au@COF. (d) $H_2O_2$ generation using Au@COF in pure water (pH=3) with different sacrificial agents under simulated sunlight irradiation, with the insert showing calculated HOMO and LUMO energies of BA. (e) Reaction mechanism of photoinduced $H_2O_2$ production and photogenerated electrons migration route using Au@COF. Reproduced with permission from ref. [71]. (f) Proposed band structure diagrams of covalent benzene-acetylene frameworks and (g) their $H_2O_2$ formation within a two-phase system. (h) Schematic drawing of photocatalytic $H_2O_2$ formation in BA/water two-phase system with weakly hydrophilic COF-TAPB-BPDA. Reproduced with permission from ref. [73].

a challenge that can be addressed through implementing a two-phase system, as illustrated in Fig. 4e. Similarly, the photo-catalyst Py-Da-COF disperses in the BA phase, with the concentration of 1 mg/mL, accompanied by the indirect 2e-ORR process, which yields $H_2O_2$ with a producing rate of 1242 µmol $h^{-1}$ $g^{-1}$, two times higher than that observed in the aqueous phase. To obtain a better dispersion of Py-Da-COF in the organic phase, the volume ratio of water/BA was decreased from 9:1 (4.5 mL/0.5 mL) to 1:1 (5 mL/5 mL), which resulted in a 37% increase in the cumulative amount of $H_2O_2$.

For the sake of synthesizing COFs with robust structures and linkages, the one-pot multi-component reactions process (MCR) is thought as a facile synthetic approach to achieve the formation of chemically stable COFs [69]. Das et al. [70] reported the one-pot synthesized COF (PMCR-1) with quinoline-linkages and the pending phenyl moieties inside the micropores, and its application in the photocatalytic $H_2O_2$ production within BA/water system. As illustrated in Fig. 5a, although PMCR-1 is able to produce high amounts of $H_2O_2$ in water with the rate of 1445 µmol $h^{-1}$ $g^{-1}$, the arrangement of BA/water two-phase system brings a marked increase of $H_2O_2$ production, which reaches 5500 µmol $h^{-1}$ $g^{-1}$ with 5 mg/mL of PMCR-1 dispersing in the water/BA (volume ratio of 10:1) medium. On the one hand, this significant improvement is attributed to the strong π-π interaction between the introduced BA molecules and the pending benzene rings within the pores of PMCR-1 (Fig. 5b), leading to the efficient hole transfer for BA oxidation. On the other hand, the hydrophobic PMCR-1 remains in the BA phase, separating from the formed $H_2O_2$ in the aqueous phase, which plays a vital role in the suppression of $H_2O_2$ decomposition. Furthermore, the authors also investigated the versatility of the selective oxidation of benzyl amines and thiols (Fig. 5b) in two-phase photocatalytic systems comprising water/benzyl amine and water/benzyl thiol. This expanded exploration broadens the scope for designing other novel binary systems in the context of photocatalytic production of $H_2O_2$ or even other photoexcited reactions.

Besides, Shang et al. [71] reported the application of carboxy-functionalized quinoline-linked COF (COF-COOH) in the BA/water dual-phase photo-reaction system for $H_2O_2$ production. The incorporation of Au nanoclusters (Au NCs) within the pores of COF-COOH enhanced the yield of $H_2O_2$. The formation of COF-O-Au bonds optimizes the energy band structure of Au@COF (Fig. 5c) and accelerates the migration efficiency of photogenerated carriers. Fig. 5d shows the photocatalytic activity of Au@COF in single- and dual-phase solutions containing different electron donors. Obviously, the amount of $H_2O_2$ produced in BA/water biphasic system achieves as high as 1893 µmol within 1 h, equivalent to the production rate of 18933 µmol $h^{-1}$ $g^{-1}$ when catalyzed by Au@COF at a concentration of 1 mg/mL, far exceeding that in single-phase system using aqueous solution of methanol, ethanol, and isopropanol. This enhanced activity attributes to the limited catalytic decomposition of $H_2O_2$ by Au@COF present in the BA phase, which enables BA molecules to be oxidized quickly by the photoexcited holes of Au@COF catalyst. The electrons of COF-COOH are easily transported to Au NCs via the COF-O-Au bridge bonds and participate in the ORR process as illustrated in Fig. 5e. Moreover, the highest HOMO energy of BA (-5.590 eV) makes it easier to lose electrons compared to other fatty alcohols and provides abundant protons for $H_2O_2$ production [72].

The aforementioned studies primarily focus on the two-phase photosynthesis of $H_2O_2$ reaction where the photocatalysts are situated in the organic phase. There has been research conducted by Yang et al. [73] according to the weakly hydrophilic acetylene-based COFs at the interface between BA and water phase. The authors designed COF-TAPB-BPDA, featuring benzene-acetylene frameworks, which exhibits more suitable band structures and stronger driving force to produce $H_2O_2$ thermodynamically than the corresponding triazine-containing COFs (COF-TAPT-BPDA and COF-TAPP-BPDA) depicted in Fig. 5f, leading to a superior $H_2O_2$ production rate of 1240 µmol $h^{-1}$ $g^{-1}$ with a concentration of 1 mg/mL in the two-phase solution

(Fig. 5g). Furthermore, the hydroxyl groups -OH of these COFs endow them with appropriate hydrophilicity with a water contact angle of about 88° shown in Fig. 5h, which allows for the efficient mass transfer of $H_2O$ and $O_2$ molecules in the water phase onto the surface of COFs in a two-phase system, thereby promoting $H_2O_2$ formation.

## 2.3. Other metallic compounds

### 2.3.1. Titanium dioxide

Titanium dioxide ($TiO_2$) has been tremendously studied as a photocatalyst for many years, owing to its high chemical stability and unique photoelectric properties. In the context of photocatalytic $H_2O_2$ production, research related to $TiO_2$ materials often involves modification with noble metals, quantum dots, organic compounds, and other semiconductor oxides to expand their light-responsive range and improve the efficiency of charge separation [11,74,75]. However, the hydroxyl groups on the surface of $TiO_2$ will be captured by the generated $H_2O_2$ molecules to form peroxide compounds (≡Ti-OOH), which causes decomposition and loss of $H_2O_2$ [76]. Therefore, considering the characteristics of two-phase systems that can spontaneously segregate $H_2O_2$ and catalysts, our group researched OPA and 2,3-dihydroxynaphthalene (2,3-DN) co-modified $TiO_2$ (DNOPA-$TiO_2$) for the two-phase system as present in Fig. 6a [77]. The grafting of 2,3-DN onto $TiO_2$ serves to enhance its capability to harness visible light, which establishes a charge transfer connection between $TiO_2$ and the resulting complex. Besides, OPA addition renders $TiO_2$ hydrophobic and makes it more stable in the BA phase, with the water contact angle of 140°, which results in the $H_2O_2$ production of 205 µmol $h^{-1}$ $g^{-1}$ under λ > 450 nm irradiation.

The preceding research demonstrates the feasibility of hydrophobic modification of $TiO_2$ and its utilization within a two-phase photo-reaction system. Moreover, to date, there exists extensive comprehension regarding the localized surface plasmon resonance (LSPR) effects of Au metal, which enables Au-deposited $TiO_2$ material to be active under visible light exposure [78–80]. However, the enhancement in the $H_2O_2$ photosynthesis process is not adequately portrayed in a single-liquid-phase reaction system due to $H_2O_2$ cleavage upon close contact with $TiO_2$ [81]. Hence, our group further investigates the advantages of a BA/water dual-phase reaction system for $H_2O_2$ yield using hydrophobic and plasmonic Au-deposited $TiO_2$ (OPA-Au/$TiO_2$) [82]. The interior reaction mechanism is depicted in Fig. 6b. Under visible light (λ > 420 nm) irradiation, the hot electrons of Au nanoparticles (Au NPs) are stimulated, with some transferring to the CB of $TiO_2$, which facilitates the conversion and utilization of photoelectrons and promotes the ORR process, yielding abundant $O_2^{\bullet-}$ intermediate products. Similarly, OPA-grafting imparts hydrophobic properties to the OPA-Au/$TiO_2$ sample, stabilizing its presence in the BA phase. Consequently, the reduction products $O_2^{\bullet-}$ migrate to the aqueous phase for $H_2O_2$ production with protons $H^+$, resulting in a productivity of 567 µmol $h^{-1}$ $g^{-1}$. In contrast, the hydrophilic Au/$TiO_2$ catalyst absorbs synthesized $H_2O_2$, leading to its decomposition into $^{\bullet}OOH$ species and a rapid decrease in $H_2O_2$ concentration over time, which validates the importance of LSPR effect of Au deposition and the two-phase setup for photosynthesis of $H_2O_2$ system.

### 2.3.2. Quantum dots

Recently, quantum dots (QDs) have emerged as promising photocatalysts owing to their capacity for strong light absorption, abundant surface reaction sites, surface functionalization and remarkable structural durability [83,84]. It is also reported that $O_2^{\bullet-}$ superoxide radicals, as important intermediates for 2e-ORR reaction to $H_2O_2$ production, could be generated on the surface of QDs under an aerobic atmosphere when exposed to visible light [85,86].

Ji et al. [87] achieved a remarkable milestone in photocatalytic $H_2O_2$ production within an oil/water two-phase system, reaching an efficiency of 61 mmol $L^{-1}$ $h^{-1}$. This exceptional result was obtained using CdSe-based core/shell QDs as depicted in Fig. 6c. In the oil phase, the
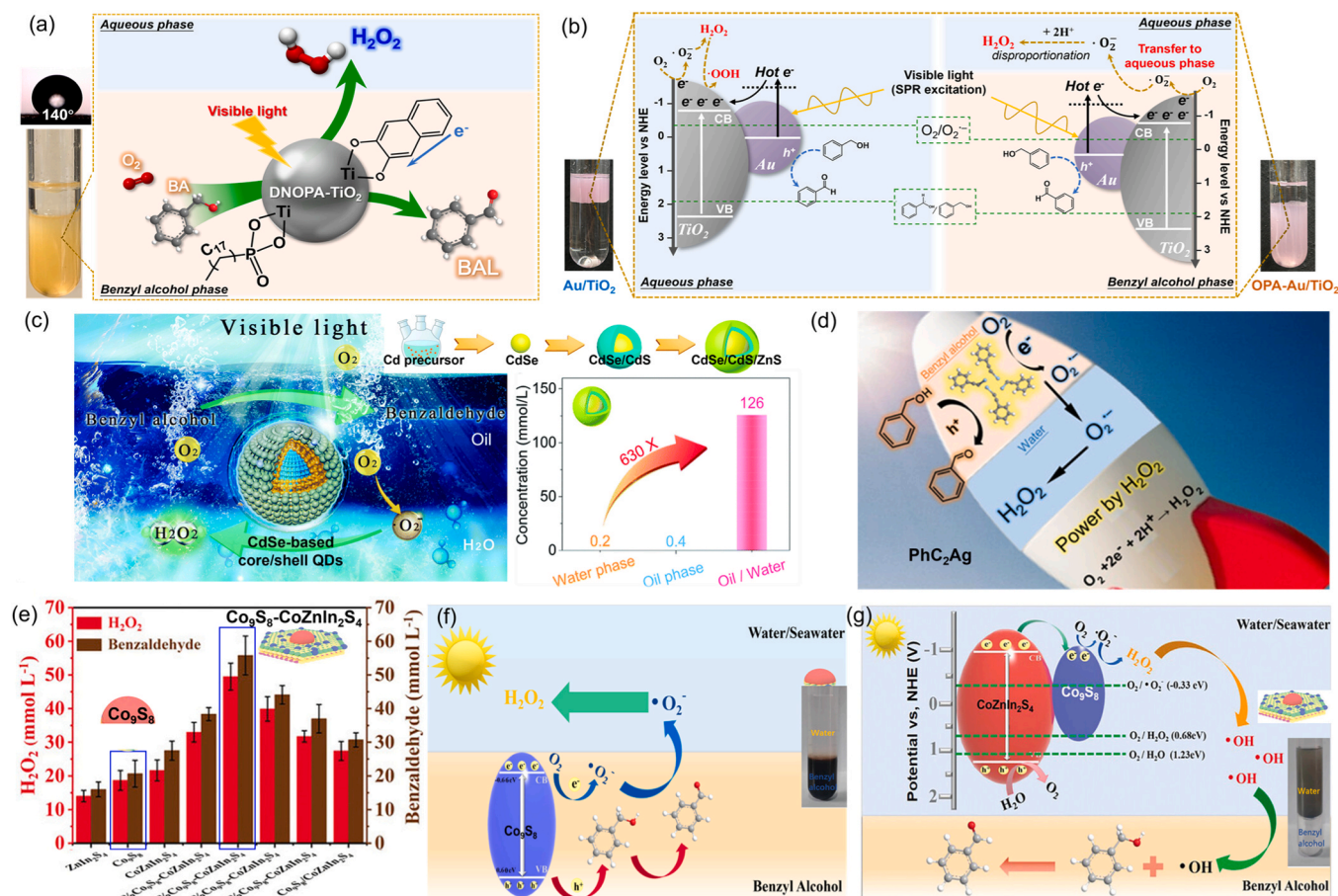
**Fig. 6.** (a) Illustration of biphasic reaction over 2,3-DN and OPA co-modified $TiO_2$ (DNOPA-$TiO_2$) materials under visible light irradiation ($\lambda > 450$ nm) [77]. (b) The photo-reaction mechanism of biphasic $H_2O_2$ synthesis using OPA-modified plasmonic Au-deposited $TiO_2$ (OPA-Au/$TiO_2$) Reproduced with permission from ref. [82]. Proposed schematic diagrams for the photocatalytic co-production of $H_2O_2$ and BAL in a two-phase system over (c) CdSe-based core/shell quantum dots and (d) Ag-based coordination polymer (PhC$_2$Ag) photocatalysts. Embedded chart of (c): Synthesis process of CdSe/CdS/ZnS and $H_2O_2$ concentration over CdSe/CdS/ZnS in single and two-phase systems. Reproduced with permission from ref. [87] and [88]. (e) $H_2O_2$ and BAL concentration of Co-based heterojunction materials in two-phase system. Proposed mechanisms of (f) hydrophobic $Co_9S_8$ and (g) hydrophilic $Co_9S_8$-CoZnIn$_2$S$_4$ in BA/water system for photocatalytic $H_2O_2$ synthesis. Reproduced with permission from ref. [89].

electrons are activated from the CdSe QDs core under visible light and react for $O_2$ reduction on the surface of the QDs. However, QDs are suffering from deterioration due to gathering or etching during irradiation, which is a challenge that can be overcome by the epitaxy of CdS. The extended CdS shell serves to eliminate the surface defects of the QD core, consequently promoting the utilization of photogenerated carriers. Unfortunately, since the easy oxidation of the CdS shell, the photostability of CdSe/CdS core-shell QDs remains inadequate. Therefore, the structure of ZnS-covered CdSe/CdS core-shell QDs (CdSe/CdS/ZnS) was eventually elaborated, considering the excellent stability and broad energy level of ZnS. Furthermore, the implementation of a BA/water two-phase system for photoinduced $H_2O_2$ production, employing CdSe/CdS/ZnS QDs, resulted in an exceptional lifting in $H_2O_2$ concentration, approximately 630 times higher than that in a single-phase system shown in the embedded chart of Fig. 6c. Such a substantial alteration serves as explicit evidence of the significant role that a two-phase system plays in the photocatalytic ORR.

### 2.3.3. Coordination polymer

Additionally, Zhu et al. [88] suggested that organometallic coordination polymer (CP) is also suitable for the development of photocatalysts for two-phase $H_2O_2$ production, owing to its flexible microstructures, tunable surface properties, and photophysical properties. As illustrated in Fig. 6d, the authors directly synthesized the hydrophobic Ag-based CP (silver phenyl acetylide, PhC$_2$Ag), rather than

post-hydrophobic modification, dispersing in the organic phase of the BA/water phase system. During the photocatalytic reaction, the electrons were activated by light irradiation to transfer to the CB of PhC$_2$Ag, participating in the reduction of $O_2$ to $O_2^{\bullet-}$ species. Similarly, $O_2^{\bullet-}$ species migrated from the BA phase to the aqueous phase for the 1e-ORR process, inhibiting the over-reduction by $O_2^{\bullet-}$ radicals and the decomposition of formed $H_2O_2$. Meanwhile, the photoinduced holes were preferentially quenched through the BA oxidation to BAL.

Notably, the authors also explored how varying the volume ratio of BA and water phases, as well as the pH values in the aqueous phase, affected the $H_2O_2$ production efficiency. A rise in the $H_2O_2$ yield was achieved as the volume of the aqueous phase decreased. Furthermore, a pH-dependent increase in the $H_2O_2$ concentration was observed with the highest activity for pH 1, attributed to the reliance of proton-coupled electron transfer processes (equations 2, 3 and 5 in Fig. 1c) on the concentration of protons.

### 2.3.4. Heterojunction

In the above discussion, the research we have summarized primarily focused on utilizing BA as a sacrificial agent to create a two-phase system with water for photocatalytic $H_2O_2$ synthesis. However, the co-production efficiency of $H_2O_2$ and BAL remains relatively low.

Recently, inspired by Isaka et al. [21] for the establishment of a BA/water system, Li et al. [89] reported the fabrication of a Co-based heterojunction photocatalyst (denoted as $Co_9S_8$-CoZnIn$_2$S$_4$), composed

of discrete $Co_9S_8$ nanoparticles deposited onto Co-based $ZnIn_2S_4$, and its utilization in BA/water system for photoinduced $H_2O_2$ production. As depicted in Fig. 6e, in contrast to the above studies, the hydrophilic $Co_9S_8$-$CoZnIn_2S_4$ existing in the aqueous phase seems to be more advantageous than hydrophobic $Co_9S_8$ in terms of $H_2O_2$ production, despite the formed $H_2O_2$ will be cleaved to $^{\bullet}OH$ radicals. Regarding this contradiction, the authors explained that the synergistic effects of Co-doping and $Co_9S_8$-$CoZnIn_2S_4$ heterojunction formation, evident in the interfacial lattice match between $Co_9S_8$ and $CoZnIn_2S_4$, mainly contributing to the photocatalytic performance.

Except for exploring the inherent properties of catalysts, the authors used the abundant seawater resource to establish the present two-phase system with BA solution. They also investigated the influence of various soluble metal cations, including $Na^+$, $Sr^+$, $K^+$, $Mg^{2+}$, and $Ca^{2+}$, on the $H_2O_2$ synthesis. It is evident that a higher concentration of metal cations enhances the $H_2O_2$ production, attributable to the electron sink effect of $Co_9S_8$-$CoZnIn_2S_4$ surrounded by metal cations, which facilitates the two-electron reduction pathways of $O_2$ [90].

In such a two-phase system, the photocatalytic reaction mechanism of $Co_9S_8$ (Fig. 6f) is similar to that of the MIL-125-$NH_2$ catalyst mentioned before. In contrast, $Co_9S_8$-$CoZnIn_2S_4$ facilitates the formation of $H_2O_2$ through the indirect 2e-ORR in the aqueous phase, and partially produced $H_2O_2$ decomposes into $^{\bullet}OH$ radicals, which are transferred into the BA phase and enable the production of BAL (Fig. 6g). This strategy of heterojunction establishment is expected to provide valuable insights for the systematic design of high-performance catalysts for the concurrent photocatalytic reactions.

## 3. Toluene/water phase

Recently, several researchers queried that the source of the summarized high $H_2O_2$ production rate in the BA/water two-phase system mostly depends on the BAL-induced auto-photocatalytic process of BA molecular for $H_2O_2$ production, rather than on the photocatalytic activity of heterogeneous photocatalysts [91–93]. As presented in Scheme 1, the BAL impurity existing in BA solution could act as a photocatalyst and contribute to the oxidation process from BA and dioxygen even under visible light irradiation ($\lambda > 420$ nm) [91]. Note, however, the autocatalysis of BA has been demonstrated to have little impact on $H_2O_2$ concentration in the overall system under visible light illumination [93, 94], as indicated by the monitored BAL and $H_2O_2$ yields in the blank contrast experiment without any photocatalysts [91]. Furthermore, several unquestioned electron donors, such as toluene and 1-octanol organic solutions, were employed to constitute the dual phases



**Scheme 1.** Proposed reaction mechanism of auto-photocatalytic oxidation process for $H_2O_2$ production in the BA-BAL system. Reproduced with permission from ref. [91].

alongside the aqueous phase.

As illustrated in Fig. 7a, the operation of a toluene/water biphasic solution brought an alternative dual-phase solvent system, in which the real performance of photocatalysts could be unambiguously evaluated. Vibbert et al. [95] developed a direct photosensitization of anthraquinone (AQ) for $H_2O_2$ production upon this biphasic system. The synthesized $H_2O_2$ was subsequently accumulated in the aqueous phase with the oxidized product of BAL remaining in the toluene phase, contributing to the on-demand $H_2O_2$ yield with sustainable solvents.

Inspired by this concept, Kumar et al. [96] constructed a cooperative reaction system of ORR process and toluene oxidation reaction for $H_2O_2$ production, which are initiated by the promising covalent triazine frameworks (CTFs) materials with tunable photophysical properties. As exhibited in Fig. 7b, the different chemical structures between thiophene-linked CTF-Th and phenyl-linked CTF-Ph result in diverse yield of $H_2O_2$ in the organic media including toluene and acetonitrile. This superiority of CTF-Th in $H_2O_2$ production is attributed to the thiophene donor linkers of CTF-Th, which support the higher interaction of thiophene with both toluene and $O_2$ molecules, based on the results of DFT binding energy calculations. Moreover, the toluene/water dual-phase setup was employed for the feasibility test and achieved the $H_2O_2$ yield of 37.8 µmol for 3 h along with a production rate of 630 µmol $h^{-1}$ $g^{-1}$ in lower layer of the dual-phase system under simulated sunlight irradiation (Fig. 7c and 7d). Although the solar to chemical conversion (SCC) efficiency of CTF-Th is quite low (0.02%), this design of toluene/water dual-phase medium simplifies the separation of toluene oxidization product of BAL and reduction product of $H_2O_2$, selectively transporting to the aqueous phase, which can produce the cleaner $H_2O_2$ solution with high purity.

## 4. Octanol/water phase

Except for aromatic alcohols, long-chain aliphatic alcohols like 1-octanol are also suitable for the construction of biphasic system for photochemical $H_2O_2$ formation, which are readily obtained from the biomass-derived chemicals [97–99].

Recently, a kind of well-designed hydrophobic ionic carbon nitride (KPHI) nanoparticles, in the form of PHI and methyl- and alkylsilane-linked silica, was achieved for the first time by Krivtsov et al. [42] and applied in the 1-octanol/water dual-liquid photocatalytic reaction system for producing $H_2O_2$. As depicted in Fig. 7e, hydrophilic KPHI and KPHI-Si (silica-modified KPHI) catalysts located in

the aqueous layer with 0.5 M HCl solution, while hydrophobized KPHI (KPHI-HMDS) dispersed in the 1-octanol organic phase. The $H_2O_2$ production behavior of hydrophilic materials upon biphasic conditions, involved in a 1-octanol/water ratio of 5:5 (mL: mL), approached stabilization during 72 h-reaction, with a final concentration of 0.05 mol $L^{-1}$ (Fig. 7f). This suggests that equilibrium was reached between the $H_2O_2$ formation and decomposition processes in the aqueous phase. In contrast, the hydrophobic material of KPHI-HMDS exhibits continuously enhanced $H_2O_2$ concentration without limitation during the long-time illustration process. Benefiting from the separation of KPHI-HMDS and formed $H_2O_2$, the photo-redox decomposition of $H_2O_2$ was inhibited and its concentration reached 0.12 mol $L^{-1}$ after reaction for 72 h.

## 5. Outlook and perspectives

In this review, current advancements in $H_2O_2$ production in two-phase reaction systems, including BA/water, toluene/water, and 1-octanol/water solution media, through light-driven photo-catalysts have been highlighted, involving MOFs, COFs, and other metal compounds. The activity performances and reaction conditions of these photo-catalysts with suitable hydrophobicity are summarized and presented in Table 1. Up to this point, we have ascertained that the implementation of a two-phase system effectively isolates the photocatalysts from the synthesized $H_2O_2$, thereby mitigating $H_2O_2$ degradation and
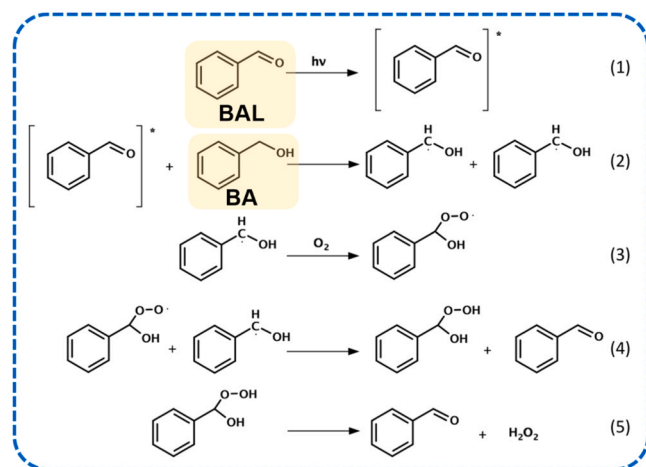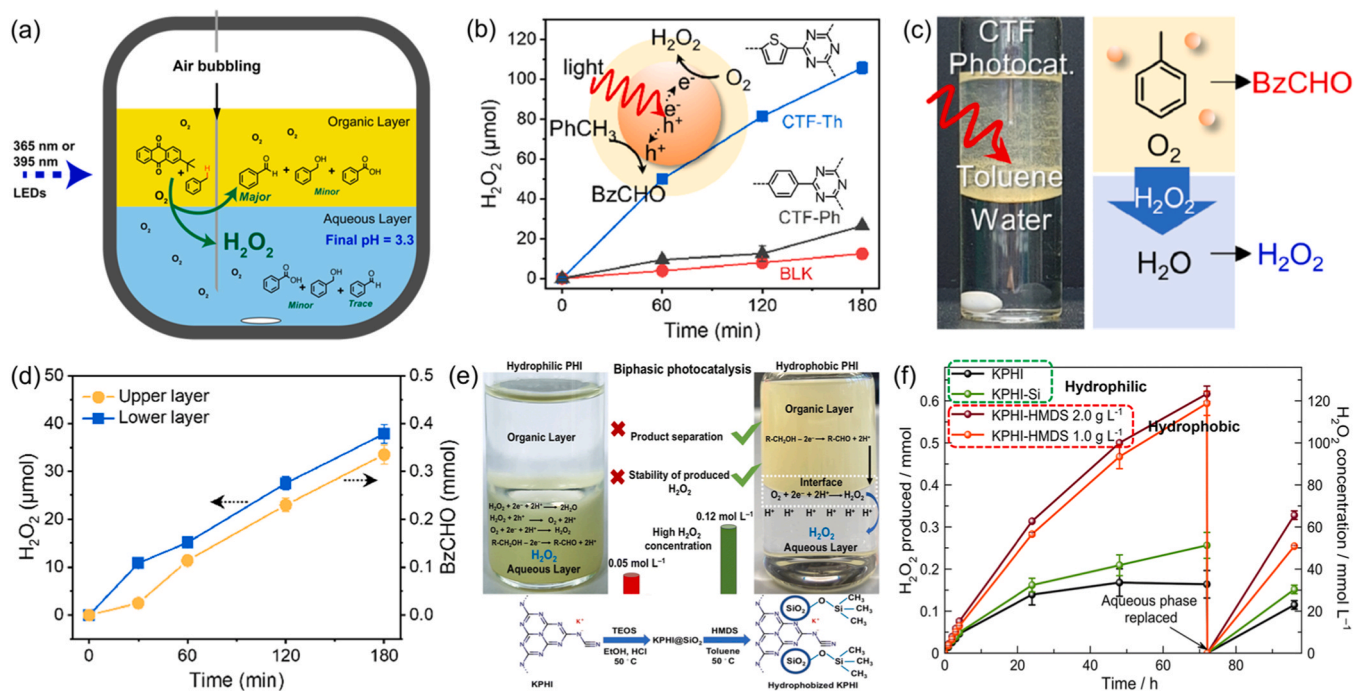
**Fig. 7.** (a) Photochemical $H_2O_2$ synthesis from anthraquinone in toluene/water biphasic solution under 365 nm LED irradiation. Reproduced with permission from ref. [95]. (b) Photocatalytic $H_2O_2$ production in the single phase composed of toluene and acetonitrile under simulated sunlight. (c) Schematic diagram of CTF-Th catalyst in the dual-phase system containing the aqueous phase and toluene phase. (d) The corresponding yield of $H_2O_2$ and BAL during the dual-phase reaction under simulated sunlight. Reproduced with permission from ref. [96]. (e) Proposed reaction mechanism of biphasic (1-octanol/water phase) photocatalysis for $H_2O_2$ synthesis using hydrophilic and hydrophobic PHI and (f) the $H_2O_2$ production under 406 nm LED light excitation. Reproduced with permission from ref. [42].

**Table 1**
Summary of reported photocatalysts for $H_2O_2$ production in two-phase systems.

| Material | Catalyst | Reaction conditions (mL: mL) | Irradiated light | $H_2O_2$ production (μmol $h^{-1}$ $g^{-1}$) | AQY/SCC | ORR pathway | Reference |
|---|---|---|---|---|---|---|---|
| MOFs | MIL-125-R7 | BA/water (5: 2) | > 420 nm (500 W, Xe lamp) | 306 | — | 1e-ORR | Isaka et al. [21] |
| | OPA/MIL-125-NH$_2$ | BA/water (5: 2) | > 420 nm (500 W, Xe lamp) | 853 | — | 1e-ORR | Kawase et al. [40] |
| | OPA/Zr$_{92.5}$Ti$_{7.5}$-MOF | BA/water (5: 2) | > 420 nm (500 W, Xe lamp) | 3733 | — | 1e-ORR | Chen et al. [22] |
| | OPA/Zr-Fe-MOF | BA/water (5: 2) | > 420 nm (500 W, Xe lamp) | 5200 | — | 1e-ORR | Chen et al. [41] |
| COFs | sonoCOF-F2 | BA/water (1: 9) | > 420 nm (300 W, Xe lamp) | 193 | 4.8% @ 420 nm | 1e-ORR | Zhao et al. [65] |
| | Py-Da-COF | BA/water (1: 9) | > 420 nm (300 W, Xe lamp) | 1242 | 4.5% @ 420 nm | 1e-ORR | Sun et al. [68] |
| | PMCR-1 | BA/water (1: 10) | > 420 nm (300 W, Xe lamp) | 5500 | 14% @ 420 nm | 1e-ORR | Das et al. [70] |
| | Au@COF | BA/water (pH=3) (5: 45) | Simulated sunlight (300 W, Xe lamp) | 18,933 | — | 1e-ORR | Shang et al. [71] |
| | COF-TAPB-BPDA | BA/water (1: 4) | > 420 nm (300 W, Xe lamp) | 1240 | — | 1e-ORR | Yang et al. [73] |
| TiO$_2$ | DNOPA-TiO$_2$ | BA/water (5: 2) | > 450 nm (500 W, Xe lamp, 100 mW cm$^{-2}$) | 205 | 0.22% @ 450 nm | 1e-ORR | Zhao et al. [77] |
| | OPA-2Au/TiO$_2$ | BA/water (5: 2) | > 420 nm (500 W, Xe lamp, 100 mW cm$^{-2}$) | 567 | — | 1e-ORR | Zhao et al. [82] |
| QDs | CdSe/5CdS/2ZnS | Oil (toluene:BA=4: 1) /water (5: 2.2) | > 420 nm (300 W, Xe lamp) | 8663 | — | 1e-ORR | Ji et al. [87] |
| CP | PhC$_2$Ag | BA/water (15: 25) | > 420 nm (10 W, LED) | 1827 | 8.62% @ 420 nm | 1e-ORR | Zhu et al. [88] |
| Heterojunction | Co$_9$S$_8$-CoZnIn$_2$S$_4$ | BA/ultrapure water (10: 25) | > 420 nm (300 W, Xe lamp, 100 mW cm$^{-2}$) | 24,750 | — | 1e-ORR | Li et al. [89] |
| CTFs | CTF-Th | Toluene/water (15: 15) | Simulated sunlight (950 W m$^{-2}$) | 630 | SCC 0.02% | 1e-ORR | Kumar et al. [96] |
| KPHI | KPHI-HMDS | 1-octanol/0.5 M HCl (5: 5) | LED 406 nm (4.2 mW cm$^{-2}$) | 1667 | 9.4% @ 406 nm | 2e-ORR | Krivtsov et al. [42] |

consumption stemming from the formation of complexes on the surface of catalysts during the reaction process. In addition, it is known that different methods of hydrophobic modification to the material affect the mass transfer efficiency of the reactant molecules on its surface and thus the $H_2O_2$ yield. Furthermore, the organic phase containing BA, toluene, or 1-octanol engages in the oxidation reaction with the photo-generated holes, yielding a distinct and valuable organic compound, BAL or 1-octanal.

This coexistence of simultaneous oxygen reduction reactions and oxidation reactions of organic molecules puts forward novel requirements and principles for catalyst design. Researchers are committed to the pursuit of optimizing photocatalytic activity and stability through the catalyst-centric perspective, including the enhancement of light absorption capabilities, augmentation of the charge transfer proficiency, and extension of the lifetimes of photogenerated electron-hole pairs. Nevertheless, additional factors, such as the catalyst concentration, the volume ratio between the aqueous and organic phases, and proton concentration (pH value) and cations in the aqueous solution, also exert significant influence on the catalytic performance within two-phase systems.

As summarized in the present review, it was universally demonstrated that in the biphasic system, higher catalyst concentrations could raise the number of active sites, while a larger proportion of organic phase volume could improve the dispersibility of catalysts within the organic layer. This allows $O_2$ and organic molecules to fully contact the catalyst particles, resulting in more efficient utilization and transportation of photoinduced electrons and holes on its surface. Furthermore, considering the spontaneous migration of the intermediate $O_2^{\bullet-}$ species to the aqueous phase during two-phase reactions, aqueous solutions with lower pH or enriched with metal cations, such as NaCl solution or seawater, are suggested as the aqueous layer in the dual-phase photocatalytic $H_2O_2$ production reaction system. This is due to the higher concentration of protons in acidic solutions can promote the reaction rate of $O_2^{\bullet-}$ disproportionation pathway (equation 5 in Fig. 1c) [48]. However, excessively acidic media may pose challenges to wastewater treatment departments and the natural environment, so it is not recommended to use it with a pH lower than 1 for this research topic.

Seawater, as the most abundant water resource on Earth (constituting over 97%), serves as an excellent and valuable alternative to deionized water. Additionally, metal cations abundant in seawater, such as $Na^+$, exhibit strong complexation with $O_2^{\bullet-}$ species, efficiently inhibiting the $H_2O_2$ decomposition process that occurs owing to redundant $O_2^{\bullet-}$ [21]. Therefore, seawater emerges as a superior medium for two-phase photocatalytic research, not only reducing the water solubility in the organic phase and effectively suppressing catalyst deactivation, but also notably enhancing efficiency in $H_2O_2$ photosynthesis, which has been verified by current literatures [21,39]. Nonetheless, attention should be paid to maintaining the volume ratio of seawater to the organic phase at or below 1:1, ensuring the high dispersion of catalysts in organic solvents.

Besides, the quest for dramatic stability necessitates a deeper contemplation of device designs and the integration of photocatalysis and electrocatalysis within a cascaded process. For example, Hao et al. [100] fabricated a membrane utilizing active MOF species and established a gas-membrane-gas which resulted in a significant enhancement in the mass transfer efficiency of $O_2$. In a parallel effort, Li et al. [61] redesigned the reaction apparatus, thereby constructing a gas-solid-liquid three-phase interface to enable the direct interaction between $O_2$ and the active sites. These designs could be well-referred and utilized in the context of the two-phase system for photocatalytic reactions to avoid the problem of low solubility and slow migration of $O_2$ within the solution. In addition, Wang et al. [101] comprehensively summarized recent progress on device designs for photo-electrochemical $H_2O_2$ production. For photocatalytic reactions in a two-phase system, the issue of limited charge transport efficiency can be effectively addressed through the incorporation of electrocatalysis.

Specifically, the introduction of an external electric field plays a dual role in enhancing charge separation and facilitating electron transfer. For example, spontaneous $O_2$ reduction and BA oxidation reactions can be designed strategically at the cathode and anode of the reaction cell, respectively, with the potential to significantly augment the co-production of both products, $H_2O_2$ and BAL.

In brief, there remains significant and promising space for the development of two-phase systems for photochemical reactions. We hope that this review provides fresh insights and conception on the future advancements in the field of sustainable $H_2O_2$ production on either photocatalysis or (photo)electrocatalysis.

## CRediT authorship contribution statement

**Yifan Zhao:** Writing – original draft, Conceptualization. **Yoshifumi Kondo:** Writing – review & editing. **Yasutaka Kuwahara:** Writing – review & editing. **Kohsuke Mori:** Writing – review & editing. **Hiromi YAMASHITA:** Writing – review & editing, Supervision, Project administration, Funding acquisition, Conceptualization.

## Declaration of Competing Interest

The authors declare the following financial interests/personal relationships which may be considered as potential competing interests: Hiromi Yamashita reports financial support was provided by Japan Society for the Promotion of Science. The corresponding author of this manuscript, Prof. Hiromi Yamashita, is one of the editorial members of this journal. If there are other authors, they declare that they have no known competing financial interests or personal relationships that could have appeared to influence the work reported in this paper.

## Data availability

No data was used for the research described in the article.

## Acknowledgements

## References

[1] J.M. Campos-Martin, G. Blanco-Brieva, J.L.G. Fierro, Hydrogen peroxide synthesis: an outlook beyond the anthraquinone process, Angew. Chem. Int. Ed. 45 (2006) 6962–6984, https://doi.org/10.1002/ANIE.200503779.

[2] W. Zhan, L. Ji, Z. Mei Ge, X. Wang, R. Tao Li, A continuous-flow synthesis of primary amides from hydrolysis of nitriles using hydrogen peroxide as oxidant, Tetrahedron 74 (2018) 1527–1532, https://doi.org/10.1016/J.TET.2018.02.017.

[3] M. Ksibi, Chemical oxidation with hydrogen peroxide for domestic wastewater treatment, Chem. Eng. J. 119 (2006) 161–165, https://doi.org/10.1016/J.CEJ.2006.03.022.

[4] R.N. Gurram, M. Al-Shannag, N.J. Lecher, S.M. Duncan, E.L. Singsaas, M. Alkasrawi, Bioconversion of paper mill sludge to bioethanol in the presence of accelerants or hydrogen peroxide pretreatment, Bioresour. Technol. 192 (2015) 529–539, https://doi.org/10.1016/J.BIORTECH.2015.06.010.

[5] B. He, Z. Wang, P. Xiao, T. Chen, J. Yu, L. Zhang, Cooperative coupling of $H_2O_2$ production and organic synthesis over a floatable polystyrene-sphere-supported $TiO_2/Bi_2O_3$ S-scheme photocatalyst, Adv. Mater. 34 (2022) 1–10, https://doi.org/10.1002/adma.202203225.

[6] Y. Kondo, K. Hino, Y. Kuwahara, K. Mori, H. Kobayashi, H. Yamashita, Lewis acid-triggered photocatalytic hydrogen peroxide production in an aluminum-based metal–organic framework, Chem. Commun. 58 (2022) 12345–12348, https://doi.org/10.1039/D2CC04454D.

[7] H. il Kim, Y. Choi, S. Hu, W. Choi, J.H. Kim, Photocatalytic hydrogen peroxide production by anthraquinone-augmented polymeric carbon nitride, Appl. Catal. B Environ. 229 (2018) 121–129, https://doi.org/10.1016/J.APCATB.2018.01.060.

[8] S. Yang, A. Verdaguer-Casadevall, L. Arnarson, L. Silvioli, V. Čolić, R. Frydendal, J. Rossmeisl, I. Chorkendorff, I.E.L. Stephens, Toward the decentralized electrochemical production of $H_2O_2$: a focus on the catalysis, ACS Catal. 8 (2018) 4064–4081, https://doi.org/10.1021/ACSCATAL.8B00217.

[9] J. García-Serna, T. Moreno, P. Biasi, M.J. Cocero, J.P. Mikkola, T.O. Salmi, Engineering in direct synthesis of hydrogen peroxide: targets, reactors and guidelines for operational conditions, Green. Chem. 16 (2014) 2320–2343, https://doi.org/10.1039/C3GC41600C.

[10] H. Hou, X. Zeng, X. Zhang, Production of hydrogen peroxide by photocatalytic processes, Angew. Chem. Int. Ed. 59 (2020) 17356–17376, https://doi.org/10.1002/ANIE.201911609.

[11] L. Zheng, H. Su, J. Zhang, L.S. Walekar, H. Vafaei Molamahmood, B. Zhou, M. Long, Y.H. Hu, Highly selective photocatalytic production of $H_2O_2$ on sulfur and nitrogen co-doped graphene quantum dots tuned $TiO_2$, Appl. Catal. B Environ. 239 (2018) 475–484, https://doi.org/10.1016/j.apcatb.2018.08.031.

[12] L. Zheng, J. Zhang, Y.H. Hu, M. Long, Enhanced photocatalytic production of $H_2O_2$ by Nafion coatings on S,N-codoped graphene-quantum-dots-modified $TiO_2$, J. Phys. Chem. C 123 (2019) 13693–13701, https://doi.org/10.1021/ACS.JPCC.9B02311.

[13] L. Zheng, X. Yu, M. Long, Q. Li, Humic acid-mediated visible-light degradation of phenol on phosphate-modified and Nafion-modified $TiO_2$ surfaces, Chin. J. Catal. 38 (2017) 2076–2084, https://doi.org/10.1016/S1872-2067(17)62951-6.

[14] K. Fuku, Y. Miyase, Y. Miseki, T. Gunji, K. Sayama, $WO_3/BiVO_4$ photoanode coated with mesoporous $Al_2O_3$ layer for oxidative production of hydrogen peroxide from water with high selectivity, RSC Adv. 7 (2017) 47619–47623, https://doi.org/10.1039/C7RA09693C.

[15] J. Lim, H. Kim, J. Park, G.H. Moon, J.J.M. Vequizo, A. Yamakata, J. Lee, W. Choi, How g-$C_3N_4$ works and is different from $TiO_2$ as an environmental photocatalyst: mechanistic view, Environ. Sci. Technol. 54 (2020) 497–506, https://doi.org/10.1021/ACS.EST.9B05044.

[16] Z. Teng, Q. Zhang, H. Yang, K. Kato, W. Yang, Y.R. Lu, S. Liu, C. Wang, A. Yamakata, C. Su, B. Liu, T. Ohno, Atomically dispersed antimony on carbon nitride for the artificial photosynthesis of hydrogen peroxide, Nat. Catal. 4 (2021) 374–384, https://doi.org/10.1038/s41929-021-00605-1.

[17] P. Ren, T. Zhang, N. Jain, H.Y.V. Ching, A. Jaworski, G. Barcaro, S. Monti, J. Silvestre-Albero, V. Celorrio, L. Chouhan, A. Rokicińska, E. Debroye, P. Kuśtrowski, S. Van Doorslaer, S. Van Aert, S. Bals, S. Das, An atomically dispersed Mn-photocatalyst for generating hydrogen peroxide from seawater via the water oxidation reaction (WOR), J. Am. Chem. Soc. 145 (2023) 16584–16596, https://doi.org/10.1021/jacs.3c03785.

[18] A. Gopakumar, P. Ren, J. Chen, B.V. Manzolli Rodrigues, H.Y. Vincent Ching, A. Jaworski, S.Van Doorslaer, A. Rokicińska, P. Kuśtrowski, G. Barcaro, S. Monti, A. Slabon, S. Das, Lignin-supported heterogeneous photocatalyst for the direct generation of $H_2O_2$ from seawater, J. Am. Chem. Soc. 144 (2022) 2603–2613, https://doi.org/10.1021/JACS.1C10786.

[19] S. Thakur, T. Kshetri, N.H. Kim, J.H. Lee, Sunlight-driven sustainable production of hydrogen peroxide using a CdS–graphene hybrid photocatalyst, J. Catal. 345 (2017) 78–86, https://doi.org/10.1016/J.JCAT.2016.10.028.

[20] P. Sun, Z. Mo, H. Chen, Y. Song, J. Liu, W. Yin, H. Dai, Z. Chen, H. Li, H. Xu, Highly efficient photosynthesis of $H_2O_2$ via two-channel pathway photocatalytic water splitting, Inorg. Chem. Front. 9 (2022) 1701–1707, https://doi.org/10.1039/d1qi01592c.

[21] Y. Isaka, Y. Kawase, Y. Kuwahara, K. Mori, H. Yamashita, Two-phase system utilizing hydrophobic metal–organic frameworks (MOFs) for photocatalytic synthesis of hydrogen peroxide, Angew. Chem. 131 (2019) 5456–5460, https://doi.org/10.1002/ange.201901961.

[22] X. Chen, Y. Kuwahara, K. Mori, C. Louis, H. Yamashita, A hydrophobic titanium doped zirconium-based metal organic framework for photocatalytic hydrogen peroxide production in a two-phase system, J. Mater. Chem. A 8 (2020) 1904–1910, https://doi.org/10.1039/C9TA11120D.

[23] Y. Kondo, K. Honda, Y. Kuwahara, K. Mori, H. Kobayashi, H. Yamashita, Boosting photocatalytic hydrogen peroxide production from oxygen and water using a hafnium-based metal–organic framework with missing-linker defects and nickel single atoms, ACS Catal. 12 (2022) 14825–14835, https://doi.org/10.1021/acscatal.2c04940.

[24] Y. Kondo, Y. Kuwahara, K. Mori, H. Yamashita, Dual role of missing-linker defects terminated by acetate ligands in a zirconium-based MOF in promoting photocatalytic hydrogen peroxide production, J. Phys. Chem. C 125 (2021) 27909–27918, https://doi.org/10.1021/ACS.JPCC.1C07735.

[25] F. Liu, P. Zhou, Y. Hou, H. Tan, Y. Liang, J. Liang, Q. Zhang, S. Guo, M. Tong, J. Ni, Covalent organic frameworks for direct photosynthesis of hydrogen peroxide from water, air and sunlight, Nat. Commun. 14 (1) (2023) 10, https://doi.org/10.1038/s41467-023-40007-4.

[26] W.K. Han, H.S. Lu, J.X. Fu, X. Liu, X. Zhu, X. Yan, J. Zhang, Y. Jiang, H. Dong, Z. G. Gu, Targeted construction of a three-dimensional metal covalent organic framework with spn topology for photocatalytic hydrogen peroxide production, Chem. Eng. J. 449 (2022) 137802, https://doi.org/10.1016/j.cej.2022.137802.

[27] Z. Chen, D. Yao, C. Chu, S. Mao, Photocatalytic $H_2O_2$ production systems: Design strategies and environmental applications, Chem. Eng. J. 451 (2023) 138489, https://doi.org/10.1016/j.cej.2022.138489.

[28] M.G. Walter, E.L. Warren, J.R. McKone, S.W. Boettcher, Q. Mi, E.A. Santori, N. S. Lewis, Solar water splitting cells, Chem. Rev. 110 (2010) 6446–6473, https://doi.org/10.1021/CR1002326.

[29] H. Cheng, J. Cheng, L. Wang, H. Xu, Reaction pathways toward sustainable photosynthesis of hydrogen peroxide by polymer photocatalysts, Chem. Mater. (2022), https://doi.org/10.1021/ACS.CHEMMATER.2C00936.

[30] X. Zeng, Y. Liu, X. Hu, X. Zhang, Photoredox catalysis over semiconductors for light-driven hydrogen peroxide production, Green. Chem. 23 (2021) 1466–1494, https://doi.org/10.1039/D0GC04236F.

[31] J. Tang, T. Zhao, D. Solanki, X. Miao, W. Zhou, S. Hu, Selective hydrogen peroxide conversion tailored by surface, interface, and device engineering, Joule 5 (2021) 1432–1461, https://doi.org/10.1016/j.joule.2021.04.012.

[32] W. Hou, Y. Li, S. Ouyang, H. Chen, J. Ye, X. Han, Y. Deng, Bifunctional hydroxyl group over polymeric carbon nitride to achieve photocatalytic $H_2O_2$ production in ethanol aqueous solution with an apparent quantum yield of 52.8% at 420 nm, Chem. Commun. 55 (2019) 13279–13282, https://doi.org/10.1039/c9cc07342f.

[33] Y. Isaka, Y. Kondo, Y. Kawase, Y. Kuwahara, K. Mori, H. Yamashita, Photocatalytic production of hydrogen peroxide through selective two-electron reduction of dioxygen utilizing amine-functionalized MIL-125 deposited with nickel oxide nanoparticles, Chem. Commun. 54 (2018) 9270–9273, https://doi.org/10.1039/C8CC02679C.

[34] Y. Kondo, Y. Kuwahara, K. Mori, H. Yamashita, Design of metal-organic framework catalysts for photocatalytic hydrogen peroxide production, Chem 8 (2022) 2924–2938, https://doi.org/10.1016/j.chempr.2022.09.007.

[35] T. Zhang, W. Schilling, S.U. Khan, H.Y.V. Ching, C. Lu, J. Chen, A. Jaworski, G. Barcaro, S. Monti, K. De Wael, A. Slabon, S. Das, Atomic-level understanding for the enhanced generation of hydrogen peroxide by the introduction of an aryl amino group in polymeric carbon nitrides, ACS Catal. 11 (2021) 14087–14101, https://doi.org/10.1021/ACSCATAL.1C03733.

[36] X. Wu, X. Zhang, S. Zhao, Y. Gong, R. Djellabi, S. Lin, X. Zhao, Highly-efficient photocatalytic hydrogen peroxide production over polyoxometalates covalently immobilized onto titanium dioxide, Appl. Catal. A Gen. 591 (2020) 117271, https://doi.org/10.1016/j.apcata.2019.117271.

[37] Y. Shiraishi, S. Kanazawa, D. Tsukamoto, A. Shiro, Y. Sugano, T. Hirai, Selective hydrogen peroxide formation by titanium dioxide photocatalysis with benzylic alcohols and molecular oxygen in water, ACS Catal. 3 (2013) 2222–2227, https://doi.org/10.1021/CS400511Q.

[38] X. Chen, X. Sheng, H. Zhou, Z. Liu, M. Xu, X. Feng, Hydrophobicity promoted efficient hydroxyl radical generation in visible-light-driven photocatalytic oxidation, Small 2310128 (2024) 1–7, https://doi.org/10.1002/smll.202310128.

[39] Z. Chen, H. Chen, K. Wang, J. Chen, M. Li, Y. Wang, P. Tsiakaras, S. Song, Enhanced $TiO_2$ photocatalytic 2e-oxygen reduction reaction via interfacial microenvironment regulation and mechanism analysis, ACS Catal. 13 (2023) 6497–6508, https://doi.org/10.1021/acscatal.3c00994.

[40] Y. Kawase, Y. Isaka, Y. Kuwahara, K. Mori, H. Yamashita, Ti cluster-alkylated hydrophobic MOFs for photocatalytic production of hydrogen peroxide in two-phase systems, Chem. Commun. 55 (2019) 6743–6746, https://doi.org/10.1039/C9CC02380A.

[41] X. Chen, Y. Kuwahara, K. Mori, C. Louis, H. Yamashita, Heterometallic and hydrophobic metal-organic frameworks as durable photocatalysts for boosting hydrogen peroxide production in a two-phase system, ACS Appl. Energy Mater. 4 (2021) 4823–4830, https://doi.org/10.1021/ACSAEM.1C00371.

[42] I. Krivtsov, A. Vazirani, D. Mitoraj, M.M. Elnagar, C. Neumann, A. Turchanin, Y. Patiño, S. Ordóñez, R. Leiter, M. Lindén, U. Kaiser, R. Beranek, Hydrophobized poly(heptazine imide) for highly effective photocatalytic hydrogen peroxide production in a biphasic fatty alcohol–water system, J. Mater. Chem. A 11 (2023) 2314–2325, https://doi.org/10.1039/D2TA08045A.

[43] H. Furukawa, K.E. Cordova, M. O`Keeffe, O.M. Yaghi, The chemistry and applications of metal-organic frameworks, Science 341 (2013) 1230444, https://doi.org/10.1126/science.1230444.

[44] S. Kitagawa, R. Kitaura, S.I. Noro, Functional porous coordination polymers, Angew. Chem. - Int. Ed. 43 (2004) 2334–2375, https://doi.org/10.1002/anie.200300610.

[45] A. Bavykina, N. Kolobov, I.S. Khan, J.A. Bau, A. Ramirez, J. Gascon, Metal-organic frameworks in heterogeneous catalysis: Recent progress, new trends, and future perspectives, Chem. Rev. 120 (2020) 8468–8535, https://doi.org/10.1021/acs.chemrev.9b00685.

[46] J.D. Xiao, Q. Shang, Y. Xiong, Q. Zhang, Y. Luo, S.H. Yu, H.L. Jiang, Boosting photocatalytic hydrogen production of a metal–organic framework decorated with platinum nanoparticles: the platinum location matters, Angew. Chem. - Int. Ed. 55 (2016) 9389–9393, https://doi.org/10.1002/anie.201603990.

[47] Y. An, H. Li, Y. Liu, B. Huang, Q. Sun, Y. Dai, X. Qin, X. Zhang, Photoelectrical, photophysical and photocatalytic properties of Al based MOFs: MIL-53(Al) and MIL-53-$NH_2$(Al), J. Solid State Chem. 233 (2016) 194–198, https://doi.org/10.1016/j.jssc.2015.10.037.

[48] Y. Nosaka, A.Y. Nosaka, Generation and detection of reactive oxygen species in photocatalysis, Chem. Rev. 117 (2017) 11302–11336, https://doi.org/10.1021/ACS.CHEMREV.7B00161.

[49] S. Kato, J. Jung, T. Suenobu, S. Fukuzumi, Production of hydrogen peroxide as a sustainable solar fuel from water and dioxygen, Energy Environ. Sci. 6 (2013) 3756, https://doi.org/10.1039/c3ee42815j.

[50] K. Mase, M. Yoneda, Y. Yamada, S. Fukuzumi, Seawater usable for production and consumption of hydrogen peroxide as a solar fuel, Nat. Commun. 7 (1) (2016) 7, https://doi.org/10.1038/ncomms11470.

[51] L. Valenzano, B. Civalleri, S. Chavan, S. Bordiga, M.H. Nilsen, S. Jakobsen, K. P. Lillerud, C. Lamberti, Disclosing the complex structure of UiO-66 metal organic framework: a synergic combination of experiment and theory, Chem. Mater. 23 (2011) 1700–1718, https://doi.org/10.1021/CM1022882.

[52] J.H. Cavka, S. Jakobsen, U. Olsbye, N. Guillou, C. Lamberti, S. Bordiga, K. P. Lillerud, A new zirconium inorganic building brick forming metal organic frameworks with exceptional stability, J. Am. Chem. Soc. 130 (2008) 13850–13851, https://doi.org/10.1021/JA8057953.

[53] Y. Han, M. Liu, K. Li, Q. Sun, W. Zhang, C. Song, G. Zhang, Z. Conrad Zhang, X. Guo, In situ synthesis of titanium doped hybrid metal–organic framework UiO-

66 with enhanced adsorption capacity for organic dyes, Inorg. Chem. Front. 4 (2017) 1870–1880, https://doi.org/10.1039/C7QI00437K.

[54] M.A. Syzgantseva, C.P. Ireland, F.M. Ebrahim, B. Smit, O.A. Syzgantseva, Metal substitution as the method of modifying electronic structure of metal-organic frameworks, J. Am. Chem. Soc. 141 (2019) 6271–6278, https://doi.org/10.1021/JACS.8B13667.

[55] D. Sun, W. Liu, M. Qiu, Y. Zhang, Z. Li, Introduction of a mediator for enhancing photocatalytic performance via post-synthetic metal exchange in metal-organic frameworks (MOFs), Chem. Commun. 51 (2015) 2056–2059, https://doi.org/10.1039/c4cc09407g.

[56] A. Santiago Portillo, H.G. Baldoví, M.T. García Fernandez, S. Navalón, P. Atienzar, B. Ferrer, M. Alvaro, H. Garcia, Z. Li, Ti as mediator in the photoinduced electron transfer of mixed-metal NH₂-UiO-66(Zr/Ti): transient absorption spectroscopy study and application in photovoltaic cell, J. Phys. Chem. C 121 (2017) 7015–7024, https://doi.org/10.1021/acs.jpcc.6b13068.

[57] C. Xu, Y. Pan, G. Wan, H. Liu, L. Wang, H. Zhou, S.H. Yu, H.L. Jiang, Turning on visible-light photocatalytic C-H oxidation over metal-organic frameworks by introducing metal-to-cluster charge transfer, J. Am. Chem. Soc. 141 (2019) 19110–19117, https://doi.org/10.1021/JACS.9B09954.

[58] K. Geng, T. He, R. Liu, S. Dalapati, K.T. Tan, Z. Li, S. Tao, Y. Gong, Q. Jiang, D. Jiang, Covalent organic frameworks: design, synthesis, and functions, Chem. Rev. 120 (2020) 8814–8933, https://doi.org/10.1021/ACS.CHEMREV.9B00550.

[59] Z. Liang, R. Shen, Y.H. Ng, Y. Fu, T. Ma, P. Zhang, Y. Li, X. Li, Covalent organic frameworks: fundamentals, mechanisms, modification, and applications in photocatalysis, Chem. Catal. 2 (2022) 2157–2228, https://doi.org/10.1016/J.CHECAT.2022.06.006.

[60] H. Wang, H. Wang, Z. Wang, L. Tang, G. Zeng, P. Xu, M. Chen, T. Xiong, C. Zhou, X. Li, D. Huang, Y. Zhu, Z. Wang, J. Tang, Covalent organic framework photocatalysts: structures and applications, Chem. Soc. Rev. 49 (2020) 4135–4165, https://doi.org/10.1039/d0cs00278j.

[61] L. Li, L. Xu, Z. Hu, J.C. Yu, L. Li, L. Xu, J.C. Yu, Z. Hu, Enhanced mass transfer of oxygen through a gas–liquid–solid interface for photocatalytic hydrogen peroxide production, Adv. Funct. Mater. 31 (2021) 2106120, https://doi.org/10.1002/ADFM.202106120.

[62] H. Wang, C. Yang, F. Chen, G. Zheng, Q. Han, A crystalline partially fluorinated triazine covalent organic framework for efficient photosynthesis of hydrogen peroxide, Angew. Chem. Int. Ed. 61 (2022) e202202328, https://doi.org/10.1002/ANIE.202202328.

[63] M. Kou, Y. Wang, Y. Xu, L. Ye, Y. Huang, B. Jia, H. Li, J. Ren, Y. Deng, J. Chen, Y. Zhou, K. Lei, L. Wang, W. Liu, H. Huang, T. Ma, Molecularly engineered covalent organic frameworks for hydrogen peroxide photosynthesis, Angew. Chem. Int. Ed. 61 (2022) e202200413, https://doi.org/10.1002/ANIE.202200413.

[64] L. Zhai, Z. Xie, C.X. Cui, X. Yang, Q. Xu, X. Ke, M. Liu, L.B. Qu, X. Chen, L. Mi, Constructing synergistic triazine and acetylene cores in fully conjugated covalent organic frameworks for cascade photocatalytic H₂O₂ production, Chem. Mater. 34 (2022) 5232–5240, https://doi.org/10.1021/ACS.CHEMMATER.2C00910.

[65] W. Zhao, P. Yan, B. Li, M. Bahri, L. Liu, X. Zhou, R. Clowes, N.D. Browning, Y. Wu, J.W. Ward, A.I. Cooper, Accelerated synthesis and discovery of covalent organic framework photocatalysts for hydrogen peroxide production, J. Am. Chem. Soc. 144 (2022) 9902–9909, https://doi.org/10.1021/jacs.2c02666.

[66] F.P. Kinik, A. Ortega-Guerrero, D. Ongari, C.P. Ireland, B. Smit, Pyrene-based metal organic frameworks: from synthesis to applications, Chem. Soc. Rev. 50 (2021) 3143–3177, https://doi.org/10.1039/D0CS00424C.

[67] G. Cheng, T. Hasell, A. Trewin, D.J. Adams, A.I. Cooper, Soluble conjugated microporous polymers, Angew. Chem. Int. Ed. 51 (2012) 12727–12731, https://doi.org/10.1002/ANIE.201205521.

[68] J. Sun, H. Sekhar Jena, C. Krishnaraj, K. Singh Rawat, S. Abednatanzi, J. Chakraborty, A. Laemont, W. Liu, H. Chen, Y. Liu, K. Leus, H. Vrielinck, V. Van Speybroeck, P. Van Der Voort, Pyrene-based covalent organic frameworks for photocatalytic hydrogen peroxide production, Angew. Chem. Int. Ed. 62 (2023) 1–9, https://doi.org/10.1002/anie.202216719.

[69] P. Das, G. Chakraborty, J. Roeser, S. Vogl, J. Rabeah, A. Thomas, Integrating bifunctionality and chemical stability in covalent organic frameworks via one-pot multicomponent reactions for solar-driven H₂O₂ production, J. Am. Chem. Soc. 145 (2023) 31, https://doi.org/10.1021/JACS.2C11454.

[70] P. Das, J. Roeser, A. Thomas, Solar light driven H₂O₂ production and selective oxidations using a covalent organic framework photocatalyst prepared by a multicomponent reaction, Angew. Chem. Int. Ed. 62 (2023), https://doi.org/10.1002/anie.202304349.

[71] Q. Shang, Y. Liu, J. Ai, Y. Yan, X. Yang, D. Wang, G. Liao, Embedding Au nanoclusters into the pores of carboxylated COF for the efficient photocatalytic production of hydrogen peroxide, J. Mater. Chem. A. 11 (2023) 21109–21122, https://doi.org/10.1039/D3TA03966H.

[72] J. Zhang, L. Zheng, F. Wang, C. Chen, H. Wu, S.A.K. Leghari, M. Long, The critical role of furfural alcohol in photocatalytic H₂O₂ production on TiO₂, Appl. Catal. B Environ. 269 (2020) 118770, https://doi.org/10.1016/J.APCATB.2020.118770.

[73] T. Yang, Y. Chen, Y. Wang, X. Peng, A. Kong, Weakly hydrophilic imine-linked covalent benzene-acetylene frameworks for photocatalytic H₂O₂ production in the two-phase system, ACS Appl. Mater. Interfaces 15 (2022) 8075, https://doi.org/10.1021/ACSAMI.2C20506.

[74] J. Wan, W. Chen, C. Jia, L. Zheng, J. Dong, X. Zheng, Y. Wang, W. Yan, C. Chen, Q. Peng, D. Wang, Y. Li, J.W. Wan, W.X. Chen, C. Chen, Q. Peng, D.S. Wang, Y. D. Li, C.Y. Jia, L.R. Zheng, J.C. Dong, X.S. Zheng, W.S. Yan, Y. Wang, Defect effects on TiO₂ nanosheets: stabilizing single atomic site Au and promoting

catalytic properties, Adv. Mater. 30 (2018) 1705369, https://doi.org/10.1002/ADMA.201705369.

[75] J. Bae, H.J. Jeon, S.H. Cho, Y. Cho, S.E. Lee, T.O. Kim, Efficiency improvement of dye-sensitized solar cells using Cu,Co/TiO₂ photoelectrodes doped by applying ultrasonic treatment, Appl. Surf. Sci. 621 (2023) 156823, https://doi.org/10.1016/j.apsusc.2023.156823.

[76] H. Sheng, H. Ji, W. Ma, C. Chen, J. Zhao, Direct four-electron reduction of O₂ to H₂O on TiO₂ surfaces by pendant proton relay, Angew. Chem. Int. Ed. 52 (2013) 9686–9690, https://doi.org/10.1002/ANIE.201304481.

[77] Y. Zhao, Y. Kondo, Y. Kuwahara, K. Mori, H. Yamashita, Hydrophobic and visible-light responsive TiO₂ as an efficient photocatalyst for promoting hydrogen peroxide production in a two-phase system, Catal. Today 425 (2024) 114350, https://doi.org/10.1016/j.cattod.2023.114350.

[78] T.H. Tan, J. Scott, Y.H. Ng, R.A. Taylor, K.-F. Aguey-Zinsou, R. Amal, Understanding plasmon and band gap photoexcitation effects on the thermal-catalytic oxidation of ethanol by TiO₂-supported gold, ACS Catal. 6 (2016) 1870–1879, https://doi.org/10.1021/acscatal.5b02785.

[79] Y. Tian, T. Tatsuma, Mechanisms and applications of plasmon-induced charge separation at TiO₂ films loaded with gold nanoparticles, J. Am. Chem. Soc. 127 (2005) 7632–7637, https://doi.org/10.1021/ja042192u.

[80] N. Sakai, Y. Fujiwara, Y. Takahashi, T. Tatsuma, Plasmon-resonance-based generation of cathodic photocurrent at electrodeposited gold nanoparticles coated with TiO₂ films, ChemPhysChem 10 (2009) 766–769, https://doi.org/10.1002/cphc.200800704.

[81] Z. Liu, X. Sheng, D. Wang, X. Feng, Efficient hydrogen peroxide generation utilizing photocatalytic oxygen reduction at a triphase iinterface, IScience 17 (2019) 67–73, https://doi.org/10.1016/j.isci.2019.06.023.

[82] Y. Zhao, H. Ge, Y. Kondo, Y. Kuwahara, K. Mori, Photosynthesis of hydrogen peroxide in a two-phase system by hydrophobic Au nanoparticle-deposited plasmonic TiO₂ catalysts, Catal. Today 431 (2024) 114558, https://doi.org/10.1016/j.cattod.2024.114558.

[83] X.B. Li, C.H. Tung, L.Z. Wu, Semiconducting quantum dots for artificial photosynthesis, 2018 28, Nat. Rev. Chem. 2 (2018) 160–173, https://doi.org/10.1038/s41570-018-0024-8.

[84] E.A. Weiss, Designing the surfaces of semiconductor quantum dots for colloidal photocatalysis, ACS Energy Lett. 2 (2017) 1005–1013, https://doi.org/10.1021/ACSENERGYLETT.7B00061.

[85] Y. Nosaka, A.Y. Nosaka, Generation and detection of reactive oxygen species in photocatalysis, Chem. Rev. 117 (2017) 11302–11336, https://doi.org/10.1021/ACS.CHEMREV.7B00161.

[86] Z. Hu, S. Liu, H. Qin, J. Zhou, X. Peng, Oxygen stabilizes photoluminescence of CdSe/CdS core/shell quantum dots via deionization, J. Am. Chem. Soc. 142 (2020) 4254–4264, https://doi.org/10.1021/JACS.9B11978.

[87] W. Ji, Z. Xu, S. Zhang, Y. Li, Z. Bao, Z. Zhao, L. Xie, X. Zhong, Z. Wei, J. Wang, High-efficiency visible-light photocatalytic H₂O₂ production using CdSe-based core/shell quantum dots, Catal. Sci. Technol. 12 (2022) 2865–2871, https://doi.org/10.1039/D2CY00269H.

[88] P. Zhu, Y. Ma, J. Li, Y. Jin, H. Cai, C. Xu, M. Huang, N. Ming chen, Hydrophobic silver-based coordination polymer for the artificial photosynthesis of hydrogen peroxide in a two-phase system, Ind. Eng. Chem. Res. 62 (2023) 982–990, https://doi.org/10.1021/ACS.IECR.2C03673.

[89] L. Li, X. Huo, S. Chen, Q. Luo, W. Wang, Y. Wang, N. Wang, Solar-driven production of hydrogen peroxide and benzaldehyde in two-phase system by an interface-engineered Co₉S₈-CoZnIn₂S₄ heterostructure, Small (2023), https://doi.org/10.1002/smll.202301865.

[90] Q. Wu, J. Cao, X. Wang, Y. Liu, Y. Zhao, H. Wang, Y. Liu, H. Huang, F. Liao, M. Shao, Z. Kang, A metal-free photocatalyst for highly efficient hydrogen peroxide photoproduction in real seawater, Nat. Commun. 12 (1) (2021) 10, https://doi.org/10.1038/s41467-020-20823-8.

[91] I. Krivtsov, A. Vazirani, D. Mitoraj, R. Beranek, Benzaldehyde-promoted (auto) photocatalysis under visible light: Pitfalls and opportunities in photocatalytic H₂O₂ production, ChemCatChem (2023), https://doi.org/10.1002/cctc.202201215.

[92] B.C. Moon, B. Bayarkhuu, K.A.I. Zhang, D.K. Lee, J. Byun, Solar-driven H₂O₂ production via cooperative auto- and photocatalytic oxidation in fine-tuned reaction media, Energy Environ. Sci. 15 (2022) 5082–5092, https://doi.org/10.1039/d2ee02504c.

[93] M.J. Pavan, H. Fridman, G. Segalovich, A.I. Shames, N.G. Lemcoff, T. Mokari, Photoxidation of benzyl alcohol with heterogeneous photocatalysts in the UV range: the complex interplay with the autoxidative reaction, ChemCatChem 10 (2018) 2541–2545, https://doi.org/10.1002/CCTC.201800284.

[94] R. Arcas, E. Peris, E. Mas-Marzá, F. Fabregat-Santiago, Revealing the contribution of singlet oxygen in the photoelectrochemical oxidation of benzyl alcohol, Sustain. Energy Fuels 5 (2021) 956–962, https://doi.org/10.1039/d0se01322f.

[95] H.B. Vibbert, C. Bendel, J.R. Norton, A.J. Moment, On-demand photochemical synthesis of hydrogen peroxide from alkylated anthraquinones, ACS Sustain. Chem. Eng. 10 (2022) 11106–11116, https://doi.org/10.1021/acssuschemeng.2c01404.

[96] S. Kumar, B. Bayarkhuu, H. Ahn, H. Cho, J. Byun, Photocatalytic H₂O₂ production in controlled oxidative environments using covalent triazine frameworks, Nano Trends 4 (2023) 100023, https://doi.org/10.1016/j.nwnano.2023.100023.

[97] T. Ishida, Y. Ogihara, H. Ohashi, T. Akita, T. Honma, M. Oji, M. Haruta, Base-free direct oxidation of 1-octanol to octanoic acid and its octyl ester over supported gold catalysts, ChemSusChem 5 (2012) 2243–2248, https://doi.org/10.1002/cssc.201200324.

[98] G. Marques, J.C. del Río, A. Gutiérrez, Lipophilic extractives from several nonwoody lignocellulosic crops (flax, hemp, sisal, abaca) and their fate during alkaline pulping and TCF/ECF bleaching, Bioresour. Technol. 101 (2010) 260–267, https://doi.org/10.1016/J.BIORTECH.2009.08.036.

[99] V.C. Corberán, M.E. González-Pérez, S. Martínez-González, A. Gómez-Avilés, Green oxidation of fatty alcohols: challenges and opportunities, Appl. Catal. A Gen. 474 (2014) 211–223, https://doi.org/10.1016/J.APCATA.2013.09.040.

[100] Y.C. Hao, L.W. Chen, J. Li, Y. Guo, X. Su, M. Shu, Q. Zhang, W.Y. Gao, S. Li, Z. L. Yu, L. Gu, X. Feng, A.X. Yin, R. Si, Y.W. Zhang, B. Wang, C.H. Yan, Metal-

organic framework membranes with single-atomic centers for photocatalytic $CO_2$ and $O_2$ reduction, Nat. Commun. 12 (2021) 2682, https://doi.org/10.1038/s41467-021-22991-7.

[101] Q. Wang, L. Ren, J. Zhang, X. Chen, C. Chen, F. Zhang, S. Wang, J. Chen, J. Wei, Recent progress on the catalysts and device designs for (photo)electrochemical on-site $H_2O_2$ production, Adv. Energy Mater. 2301543 (2023) 1–27, https://doi.org/10.1002/aenm.202301543.